Novel behaviors in fermion systems with point-like Fermi surfaces and singular interactions

William F. Shively

A dissertation submitted to the faculty of the University of North Carolina at Chapel Hill in partial fulfillment of the requirements for the degree of Doctor of Philosophy in the Department of Physics & Astronomy.

Chapel Hill

2006

Approved:
D. V. Khveshchenko, Advisor
J. Engel, Reader
H. Karwowski, Reader
Y. J. Ng, Reader
S. Washburn, Reader

ABSTRACT

WILLIAM F. SHIVELY: Novel behaviors in fermion systems with point-like Fermi surfaces and singular interactions

(Under the Direction of D. V. Khveshchenko)

Modern condensed matter physics owes much of its success to Fermi liquid theory. In recent times, however, the study of strongly correlated particle systems is opening up all-new territory in many-body physics. A peculiar class of such systems, that of nodal fermions, is characterized by the quasiparticle density of states vanishing at the point-like Fermi surface and long-range inter-particle interactions surviving unscreened. In the first part, I discuss fermion pairing in one such system, 2D graphene. By solving the gap equation for the excitonic order parameter, I obtain values of critical interaction strength for a variety of power-law interactions and densities of states. Furthermore, these results are then used to compute the respective free energies and analyze possible phase transitions. In the second part, I discuss the effects of lattice disorder and impurities on the density of states in nodal fermion systems. These results and predictions will be of interest to a broad range of physical problems involving nodal fermions, and can be tested in a variety of experimental directions.

ACKNOWLEDGMENTS

I would like to thank Dr. Dmitri Khveshchenko for his mentorship over the last two years. I would also like to thank Dr. Hugon Karwowski and the Dept. of Physics & Astronomy of UNC Chapel Hill for their support throughout my graduate education.

Lastly, thanks to all my family and friends, both here and passed on, for their undying support.

William F. Shively

July 19, 2006

To my Parents,
Ken & Carol

CONTENTS

LIST OF FIGURES

Chapter 1

Introduction

1.1 Fermi liquids and non-Fermi liquid candidates

Over the last fifty years, Fermi liquid theory has served physicists well in describing many condensed matter systems. It is perhaps surprising how many phenomena can be described in terms of weakly correlated many-body theory, in which electron-electron interactions are largely ignored. However, while Fermi liquid theory describes a subset of many-body phenomena quite well, other phenomena fall squarely outside of this region.

In more recent times, one of the prominent directions in modern condensed matter physics is that of **strongly correlated** electron theories. Such systems are nonperturbative in nature, and being as such, traditional Fermi liquid techniques break down. One such example can be found in effectively 2-dimensional (hereafter 2D) monolayers of graphite, or *graphene*. Graphene is an example of a degenerate semimetal, the electronic structure of which harbor regions where the conduction and valence bands meet at a point. In these vicinities the Fermi surface consists of isolated Fermi points ("nodes"), at which the excitation density of states (DOS) vanishes and strongly correlated phenomena occur, having dramatic effects on the electronic properties of the system as a whole.

For years, theorists have made predictions and conjectures about what new physics might occur in these zones [4, 7, 8, 9, 10, 11, 12, 3, 13]. All sorts of parallels have been made with other areas of physics: (2+1)-D electrodynamics, chiral field theories, non-BCS kinematics, to name a few. Furthermore, as advances have been made in fullerenes and carbon nanotubes [14, 15] – the latter of which can be thought of as a sheet of graphene rolled into a tube – great interest has grown over the electronic properties of such systems. A fuller understanding of these properties would not only further our knowledge of fundamental properties of nature,

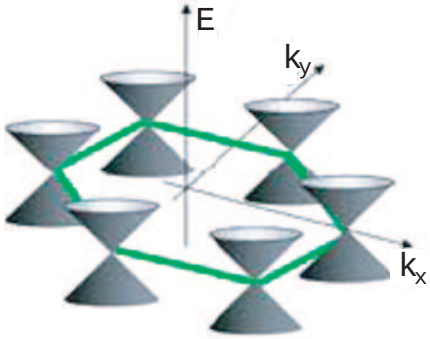

Figure 1.1: The low-energy dispersion relations near the Dirac points in the graphene Brillouin zone. (Reproduced from [1])

but it could also result in unconceived applications in materials science.

Recently, new techniques have been developed for creating very clean samples of just a few graphitic monolayers (c.f., [16, 17, 18] and references therein, and in the papers that follow). This has led to an explosion of research, some of the most recent major developments of which are discussed here. One of the most significant is that this has allowed direct experimental observations of the quantum Hall effect (QHE) and Berry's phase in graphite [19, 1, 20]. Although previous studies did observe indications of Landau level (LL) formation, the QHE was not observed, probably due to the low mobility of carriers in the samples [21, 22, 23]. Kim *et al.* [1] extracted graphene samples with far higher mobilities ($> 10^4 \mathrm{cm}^2 V^{-1} s^{-1}$), allowing them to probe deep into the magnetic quantum limit and investigate various transport phenomena. In so doing, they were able to probe the physics around the Dirac point directly, controlling the charge density via the gate voltage, V_g.

Although the QHE has been observed in many other materials, in graphene it is distinctly different, as the quantization condition for the transverse resistance,

$$R_{xy}^{-1} = \pm g_s (n + 1/2) e^2/h,$$

is shifted by a half-integer and hence is antisymmetric. (Here n is a positive integer, the spin and sublattice degeneracy $g_s = 4$, $h/e^2 \approx 25812.8\Omega$, $h = 2\pi\hbar$, and $\pm$ stands for electrons and holes, respectively.) This half-integer shift is a signature of Dirac particles [24], and is directly due to pseudo-relativistic LLs [25, 26, 27] and the carriers behaving "relativistically" with a (fictitious) effective mass $m_c = E_F/v_F^2$ at the Dirac point. This opens up many interesting issues concerning mesoscopic transport in such systems and could potentially have applications in carbon-based electric and magnetic field-effect devices [22].

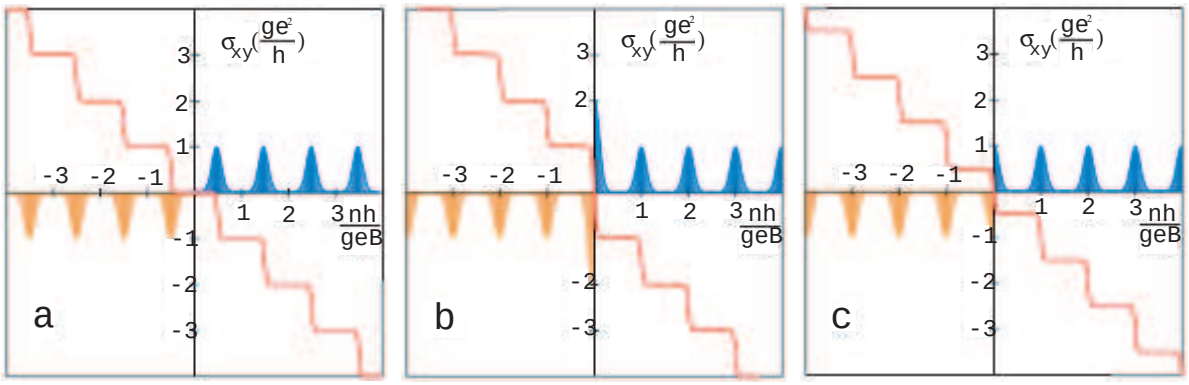

Figure 1.2: Plateaus in Hall conductivity σ_{xy} for the three types of the integer quantum Hall effect (IQHE) (reproduced from [2]). *right to left*: conventional IQHE in 2D semiconductor systems; IQHE in bilayer graphene; IQHE for massless Dirac fermions in single-layer graphene. The plateaus occur at integer multiples of ge^2/h, where e^2/h is the conductance quantum and g the system degeneracy. Note the zero-level plateau is missing in the IQHE in bilayer graphene as it is in the relativistic single-layer IQHE. The Landau levels corresponding to electrons (blue) and holes (orange) are shown. B is the magnetic field and $\phi_0 = h/e$ is the flux quantum.

Geim *et al.* [21] observed the electric field effect – allowing one to control the carrier concentration in a semiconductor device via an externally applied voltage – in naturally occurring 2D few-layer graphene. Different from multilayer graphene or bulk graphite, "few-layer graphene" (FLG) refers to devices consisting of as few as just one to three atomic layers, all of which are observed to behave in a manner essentially identical to a 2D semimetal. Pushing even further to single- and double-layer graphene, this group later discovered [2] that double-layer graphene displays an unconventional QHE (see fig.1.2) and Berry's phase, due to the massless Dirac fermions characteristic of either single layer coupling together into a novel kind of massive *chiral* quasiparticle. Such quasiparticles are similar to those in the conventional QHE in that they display parabolic dispersion and finite effective mass, but significantly different in that they also acquire a Berry's phase of 2π over cyclotron trajectories. This remains an open issue to be addressed by theorists.

Most recently, following on the heels of these results, de Heer *et al.* [28] conducted a magneto-spectroscopy study of the optical properties of ultrathin epitaxial graphite layers and directly measured the energy dispersion of electrons in systems consisting of just a single graphene monolayer or a few weakly coupled layers. As predicted by theory (c.f., [4, 7] and Ch.2 below), direct evidence was found that the free charge carriers in epitaxial graphite do, in fact, behave as massless Dirac particles with a "relativistic" (linear) energy $E_p = \pm\tilde{c}|\vec{p}|$, with a measured velocity $\tilde{c} \approx (1.03 \pm 0.01) \times 10^6 m/s$. Furthermore, they also observed a class

of transitions outside of standard 2D electron gas (2DEG) theory, from filled hole states to empty electron states: particle-antiparticle creation and annihilation events in Dirac formalism. This work marks the first known measurement of Dirac spectra in condensed matter systems.

Thanks to developments in spintronics, etc., there remains continued interest in the magnetic properties of nonmetallic compounds, including pyrolytic graphite and other degenerate semimetals. Such systems could harbor a latent excitonic instability, from which the compound would undergo a phase transition into a (possibly weak, but robust) ferromagnetic state [29, 30]. Previously, it was believed that one such degenerate semimetal, the hexaborides, could be a candidate for such a ferromagnet [31, 32, 33, 34, 35, 36], but they were later disqualified [37] on the grounds that the apparent ferromagnetism was actually due to *extrinsic* contamination from ferromagnetic compounds containing Fe and Ni, rather than to the intrinsic electronic qualities of the hexaboride itself. However, reports of weak ferromagnetism in some graphitic samples [38, 20] are still unexplained, and remain open possibilities.

Degenerate semimetals are an example of a broader class of very different nodal fermion systems. Other examples include p-wave superfluids (e.g. He_3), d-wave superfluids (e.g. cuprates), and f-wave charge density wave (CDW) insulators (e.g. dichalcogenides). A considerable amount of physical phenomena are universal to all such systems, and symmetries should be seen in the physics of these otherwise very different physical systems. I'll return to this point in chapter five.

New challenges lie ahead for theorists to explain and predict new phenomena, and to do so will require non-traditional techniques. Up until now, physicists have resorted to various simplifications or numerical approximations as a way of getting around the nonperturbative nature of such strongly coupled phenomena. In this work, I attempt to show new analytical approaches to confronting strongly-correlated physics directly, accommodating nonperturbative phenomena that have been left unaccounted for in the past. I will not simply focus on one particular system; rather, I will examine a whole host of systems with various DOSs and effective inter-particle interactions, all related to each other by harboring a formally similar order parameter relation. After some preliminary background details (chapter two), in chapter three I will focus on pairing interactions between fermions and associated quantum phase

transitions. In chapter four, I will explore the effects lattice disorder and impurities can have on the kinematics of such systems. Finally, in chapter five I will discuss what repercussions and applications these new results have in a variety of strongly-correlated nodal fermion systems.

Chapter 2

Strongly Coupled Phenomena in Graphene: Beyond Fermi Liquid Theory

As discussed in the previous chapter, nodal fermion systems are those in which the conduction and valence bands touch, causing the DOS for the quasiparticle Fermi surface to vanish. In this vicinity, long-ranged interactions remain unscreened, whether they be bare Coulomb interactions or those mediated by soft collective modes proliferating near an emerging instability. Degenerate semimetals, such as graphite or bismuth, are known to harbor nodal fermion systems. Illustrating semimetals in general, we will look specifically at planar graphene [4, 7, 8, 9, 10, 11, 12, 3]. We begin with some basic properties.

2.1 Electronic Structure in Degenerate Semimetals

Planar graphene has a honeycomb lattice structure, as depicted in fig.2.1, consisting of two interpenetrating triangular sublattices (labeled A and B), with one lattice point of each type in each Brillouin zone. Quasiparticle excitations have momenta labeled $i = 1, 2$ with respect to either sublattice, creating two effective fermion "flavors." The conduction and valence bands touch at two inequivalent conical K points located at the corners of the hexagonal Brillouin zone, and it is at these nodes that the low-energy quasiparticles excitations have a linear dispersion relation $E^{(0)}_{\mathbf{p}} = \pm v\mathbf{p}$, the velocity v being proportional to the width of the electronic π band $t \approx 2.4$ eV [4, 7]. In the limit that all lattice strain vanishes, these

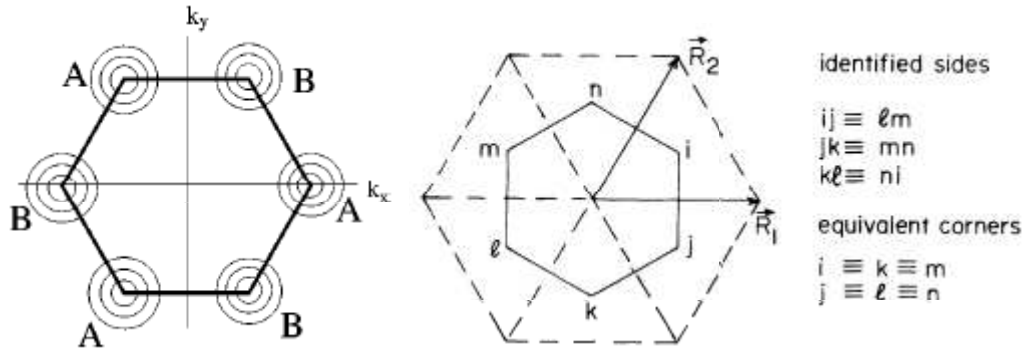

Figure 2.1: Planar graphene honeycomb lattice (left) and Brillouin zone (right) (reproduced from [3] and [4]).

two points are exactly degenerate.

The formal similarity between fermions in lattice gauge theories and the tight-binding description of electrons in crystals [4, 10] leads to a free-field theory on the graphene lattice. Thus, we will be confining ourselves to such descriptions of graphene.

In this approximation, we are actually diagonalizing the Hamiltonian

$$H = \gamma \sum_{\langle i,j \rangle} a_i^+ a_j \tag{2.1}$$

where the sum is over nearest-neighbors i, j and the operators a_i and a_j satisfy

$$\{a_i, a_j\} = \left\{a_i^+, a_j^+\right\} = 0 \qquad\qquad \left\{a_i, a_j^+\right\} = \delta_{ij} \tag{2.2}$$

In the case of graphite, each site of the honeycomb lattice yields one electron to the Fermi sea.

Using the notation presented in [10], we can think of the wavefunctions as being composed of two identical orbitals $\phi_\bullet$ and $\phi_\circ$, localized around the locations of each of the two atoms in the primitive cell. Constructing the eigenstate

$$|\Psi\rangle = \sum_{i\circ} c_\circ e^{i\mathbf{k}\cdot\mathbf{r_i}} a_i^+ |0\rangle + \sum_{i\bullet} c_\bullet e^{i\mathbf{k}\cdot\mathbf{r_i}} a_i^+ |0\rangle \,, \tag{2.3}$$

if we act with the Hamiltonian (2.1)

$$\begin{aligned} H|\Psi\rangle &= \gamma \sum_{\langle i,j \rangle} a_i^+ a_j \sum_{i\bullet} c_\bullet e^{i\mathbf{k}\cdot\mathbf{r}_i} a_i^+ |0\rangle + \gamma \sum_{\langle i,j \rangle} a_i^+ a_j \sum_{i\circ} c_\circ e^{i\mathbf{k}\cdot\mathbf{r}_j} a_i^+ |0\rangle \\ &= \gamma \sum_j e^{i\mathbf{k}\cdot\mathbf{u}_j} \sum_{i\bullet} c_\circ e^{i\mathbf{k}\cdot\mathbf{r}_i} a_i^+ |0\rangle + \gamma \sum_j e^{i\mathbf{k}\cdot\mathbf{v}_j} \sum_{i\circ} c_\bullet e^{i\mathbf{k}\cdot\mathbf{r}_i} a_i^+ |0\rangle \,. \end{aligned} \tag{2.4}$$

Here, $\{\mathbf{u}_j\}$ is a triad of vectors pointing in the direction of the nearest neighbors of a $\bullet$ point, $\{\mathbf{v}_j\}$ the triad made of their respective opposites, and

$$\beta = \int d^2r \bar{\phi}_\bullet(\mathbf{r}) H \phi_\bullet(\mathbf{r}) = \int d^2r \bar{\phi}_\circ(\mathbf{r}-\mathbf{d}) H \phi_\circ(\mathbf{r}-\mathbf{d}) \tag{2.5}$$

$$\gamma = \int d^2r \bar{\phi}_\bullet(\mathbf{r}) H \phi_\circ(\mathbf{r}-\mathbf{d}) = \int d^2r \bar{\phi}_\circ(\mathbf{r}-\mathbf{d}) H \phi_\bullet(\mathbf{r}-\mathbf{d}-\mathbf{v}_i). \tag{2.6}$$

Thus, if $c_\bullet$ and $c_\circ$ are solutions to the eigenvalue problem

$$\begin{pmatrix} 0 & \gamma \sum_j e^{i\mathbf{k}\cdot\mathbf{u}_j} \\ \gamma \sum_j e^{i\mathbf{k}\cdot\mathbf{v}_j} & 0 \end{pmatrix} \begin{pmatrix} c_\bullet \\ c_\circ \end{pmatrix} = E_k \begin{pmatrix} c_\bullet \\ c_\circ \end{pmatrix}, \tag{2.7}$$

the eigenstate (2.3) is an eigenvector of H, and

$$E_k = (\bar{c}_\bullet, \quad \bar{c}_\circ) \begin{pmatrix} \beta & \gamma \sum_j e^{ia\mathbf{k}\cdot\mathbf{u}_j} \\ \gamma \sum_j e^{ia\mathbf{k}\cdot\mathbf{v}_j} & \beta \end{pmatrix} \begin{pmatrix} c_\bullet \\ c_\circ \end{pmatrix}. \tag{2.8}$$

The solution to the eigenvalue equation is

$$E_{\mathbf{k}} = \pm\gamma \sqrt{1 + 4\cos^2 \frac{\sqrt{3}}{2} k_x + 4 \cos \frac{\sqrt{3}}{2} k_y \cos \frac{3}{2} k_y} \tag{2.9}$$

The reciprocal lattice vectors are given by

$$\mathbf{K}_1 = \frac{2\pi}{\sqrt{3}} \mathbf{e}_x + \frac{2\pi}{3} \mathbf{e}_y \qquad\qquad \mathbf{K}_2 = \frac{4\pi}{3} \mathbf{e}_y. \tag{2.10}$$

The primitive cell of the reciprocal lattice (a hexagon), which consists of only the points that reach the Fermi level, are the six vertices

$$\begin{aligned} k_x &= \pm \tfrac{4\pi}{3\sqrt{3}} \qquad k_y = 0 \\ k_x &= \pm \tfrac{2\pi}{3\sqrt{3}} \quad k_y = \pm \tfrac{2\pi}{3}. \end{aligned} \tag{2.11}$$

Because of the symmetry of the lattice, only two of these points are independent, hence we have our two K Fermi points.

Taking the continuum limit in order to study low energy excitations,

$$\mathbf{k} = \frac{4\pi}{3\sqrt{3}} \mathbf{e}_x + \delta k \tag{2.12}$$

and

$$\mathcal{H} \equiv \begin{pmatrix} 0 & \gamma \sum_j e^{ia\mathbf{k}\cdot\mathbf{u}_j} \\ \gamma \sum_j e^{ia\mathbf{k}\cdot\mathbf{v}_j} & 0 \end{pmatrix} \approx -\frac{3}{2} \gamma a \begin{pmatrix} 0 & \delta_x + i\delta k_y \\ \delta_x - i\delta k_y & 0 \end{pmatrix} + \mathcal{O}\left((a\ \delta k)^2\right) \tag{2.13}$$

Naïvely scaling,

$$\lim_{a\to 0} \mathcal{H}/a = -\frac{3}{2}\gamma\sigma^{\mathbf{T}}\cdot\delta\mathbf{k} \tag{2.14}$$

which is the Dirac operator in 2D. Hence, the quasiparticle excitations behave as pseudo-relativistic Dirac particles, with a linear dispersion $E_p = \pm v_F p$, where the speed of light c has been replaced by the Fermi velocity $v_F \approx 2\times 10^6 m/s$.

2.2 Hamiltonian

We can formulate the quasiparticle excitations in terms of the Bloch states on the two sublattices by writing them as a pair of two-component Weyl matrices (one for each "flavor"), $\psi_{i\sigma}$, where σ is a spin index. We can further combine this pair together into one four-component Dirac spinor $\Psi_\sigma = (\psi_{1\sigma}, \psi_{2\sigma})$ [39], and treat the number of species N as an adjustable parameter. (In the physical case, $N = 2$.) Then the free quasiparticle Hamiltonian can be written as

$$H_0 = iv_F \sum_{\sigma=1}^{N} \int_{\mathbf{r}} \bar{\Psi}_\sigma \left[\hat{\gamma}_1\nabla_x + \hat{\gamma}_2\nabla_y\right]\Psi_\sigma \tag{2.15}$$

The Coulomb interaction contribution can be written as

$$H_C = \frac{v_F}{4\pi}\sum_{\sigma,\beta=1}^{N}\int_{\mathbf{r}}\int_{\mathbf{r}'} \bar{\Psi}_\sigma(\mathbf{r}')\,\Psi_\sigma(\mathbf{r}')\,\frac{g}{|\mathbf{r}-\mathbf{r}'|}\bar{\Psi}_\beta(\mathbf{r})\,\Psi_\beta(\mathbf{r}) \tag{2.16}$$

where $\bar{\Psi}_\sigma = \Psi_\sigma^\dagger\hat{\gamma}_0$ and the reducible representation of the 4×4 γ-matrices is written in terms of the Pauli matrices τ_i as $\hat{\gamma}_{0,1,2} = (\tau_3, i\tau_2, -i\tau_1)\otimes\tau_3$. (See also App.A.)

In the particle-hole representation, the inverse fermion Green function reads

$$\hat{G}^{-1}(\omega,\mathbf{p}) = \omega - \mu - \hat{\tau}_3\xi_p + \hat{\tau}_1\Delta_p \tag{2.17}$$

where $\hat{\tau}_i$ is the triplet of the Pauli matrices acting in the particle-hole space, μ is the chemical potential, and Δ_p is the anticipated p-dependent gap function. The gap function describes the spatially uniform pairing in the particle-hole ("Peierls") channel caused by a long-ranged generalized repulsive potential. For the Coulomb interaction above, this is given in terms of the Fourier transform

$$U^{(0)}(\mathbf{q}) = g_0/q. \tag{2.18}$$

We can further generalize this to account for a *general* effective long-range (Coulomb-like) interaction by writing

$$U^{(0)}(\mathbf{q}) = g_0/q^{\eta\alpha} \tag{2.19}$$

where α and η are real adjustable parameters, η being determined by the generalized dispersion relation $\xi_p \propto p^\eta$. We may generalize the power-law density of states (DOS) $\nu(\epsilon) \propto \epsilon^\beta$, where β is a real adjustable parameter, related to η and the effective dimension of the the system via $\beta = D/\nu - 1$ [40]. This will be discussed more in chapter three. [1]

When the nodal fermion polarization $\Pi(\omega, \mathbf{q})$ is taken into account in the above long-range interaction (2.19), the renormalized effective interaction is

$$U(\omega, \mathbf{q}) = \frac{g_0}{q^{\eta\alpha} + g\Pi(\omega, \mathbf{q})} \tag{2.20}$$

Letting Λ be the span of the Brillouin zone, for low momenta $p \ll \Lambda$ and even lower frequencies ($\omega/q^\eta \to 0$ and $q \to 0$), the one-loop polarization behaves as $\Pi(0, \mathbf{q}) \propto q^{D-\eta}$. This implies that, under the condition $\alpha \leq \beta$, the effective interaction (2.20) retains its bare form. It will be adjusted by a finite renormalization of the coupling constant $g_0 \to g_0 \left[1 + g_0\Pi(0, \mathbf{q})/q^{\eta\alpha}\right]^{-1}\big|_{q\to 0}$ and an additional frequency dependence at the limit $\alpha = \beta$, but these effects are of lesser degree. However, if $\alpha > \beta$, the overscreened effective interaction (2.20) takes on a universal form governed by the fermion polarization, thus giving rise to behavior that is qualitatively similar to that occurring on the line $\alpha = \beta$.

2.3 Schwinger-Dyson, Gap Equation

The gap equation is given by the $\hat{\tau}_1$-component of the Schwinger-Dyson equation for the above fermion quasiparticle propagator (2.17):

$$G^{-1}(\omega_m, \vec{p}) = G_0^{-1}(\omega_m, \vec{p}) - T \sum_{n=-\infty}^{\infty} \int \frac{d^2k}{(2\pi)^2} \gamma^0 G(\omega_n, \vec{k}) \gamma^0 U(\vec{p} - \vec{k}) \tag{2.21}$$

Wave function renormalization is a next-to-leading order effect in the $1/N_f$ expansion, thus we can neglect it [41]. Also, since we are dealing with a nonrelativistic model, we can assume that the retardation effects of the gauge field are negligible ("instantaneous exchange approximation").

[1] We could seek a more general spatially-variable solution, which would then lead to investigating possible Fulde-Ferrel-Larkin-Ovchinnikov (FFLO) states, in which the order parameter demonstrates periodic spatial variations. However, preliminary results suggest that such states may only provide alternatives to the uniform ground state in the vicinity of $\mu \approx \mu_c$, opening the possibility of a sequence (at least, two) transitions that might occur in this region.

Thus, we arrive at the gap equation

$$\Delta(\mathbf{p}) = \sum_{\mathbf{q},\mp} U\left(0, \mathbf{p}-\mathbf{q}\right) \frac{(\mp)\,\Delta(\mathbf{q})}{2E_q} \theta\left(\mu \mp E_q\right) \tag{2.22}$$

where $E_{\mathbf{q}} = \sqrt{\chi_{\mathbf{q}}^2 + \Delta_{\mathbf{q}}^2}$ is the quasiparticle energy, and the sum is taken over all the occupied states in both the valence ($\Omega = -E_{\mathbf{q}}$) and conduction ($\Omega = E_{\mathbf{q}}$) bands. The occupation factor $\theta(\mu \mp E_q)$ sets a lower limit of momentum integration. For any $\alpha > 0$, a nontrivial momentum dependence of the integral kernel in eq.(2.22) rules out the possibility of the standard BCS solution $\Delta_{\mathbf{q}} = const.$

Solving the gap equation for arbitrary p, μ would reveal the dynamics and phases for these nodal systems. However, solutions for arbitrary α, β are nearly impossible to obtain directly. That said, we may overcome these difficulties if we instead employ an approximate analytical technique, the "bifurcation approximation". It is that to which we now turn.

Chapter 3

Excitonic Pairing in Nodal Fermionic Systems

3.1 The Bifurcation Approximation

It is conceivable that in graphene such a scenario as a novel form of excitonic instability could arise, resulting from the opening of a gap in the quasi-2D electronic spectrum. Moreover, such an instability would manifest itself through the onset of an insulating charge density wave (CDW) [39].

Such a transition is interaction driven. Previous investigations [42, 43] focused chiefly on short-ranged Hubbard-like intersite and nearest-neighbor repulsive interactions, ignoring longer-ranged interactions that can be present in poorly screened semimetals. On the other hand, others [11, 9, 12] focused specifically on the long-ranged Coulomb interactions and their renormalization, and concluded that, because the renormalized coupling monotonously decreases for low energies, it therefore could not cause an instability in the gapless paramagnetic ground state of graphite. However, in trying to explain the experimentally observed linear energy dependence of the quasiparticle damping [44, 45], their estimated bare coupling constant ($g \geq 10$) is too large and calls their results into question.

As a different approach, Khveshchenko [39] proposed investigating the nature of the ground state and quasiparticle spectrum by employing a *nonperturbative* method in solving a nonlinear equation for the electron Green function. One may approach this numerically (c.f., Khveshchenko and Leal [46]) or analytically, via some approximation (c.f., Khveshchenko and

Shively [40]). It is the latter method we take up here.

The quasiparticles themselves are confined to the 2D plane, whereas the Coulomb interaction between them is described by 3D gauge fields allowed to propagate into the 3D bulk. The dynamical gap for $T = 0$ and $\mu = 0$, with a linear density of states (DOS) ($\nu(\epsilon) \propto \epsilon$) and energy dispersion ($\xi_p \propto p$), and bare interaction $U^{(0)}(\vec{q}) = \lambda/q$ can be written as

$$\Delta_p = \lambda \int dq \frac{q\Delta_q K(p,q)}{\sqrt{q^2 + (\Delta_q/v_F)^2}} \tag{3.1}$$

where the (approximate) expression for the kernel

$$K(p,q) = \frac{\theta(p-q)}{p} + \frac{\theta(q-p)}{q}, \tag{3.2}$$

and the coupling

$$\lambda = \frac{e^2}{2(\epsilon_0 v_F + \pi e^2 N_f/4)}. \tag{3.3}$$

As discussed in the previous chapter, we can generalize the above technique to account for arbitrary energy dispersions (parameterized by η), DOS (β), and effective long-ranged interactions (α and η). ((3.1) above corresponds to $\alpha = \beta = \eta = 1$.) Solving such a self-consistent equation for general α and β is daunting, if not entirely impossible. However, a technique proposed by Miransky *et al.* [41] allows us to circumnavigate this difficulty by turning the above integral equation into a *differential equation*, provided that our momenta $\Delta \ll p \sim \Lambda$. This technique was used for specific α, β values in previous papers (c.f. eq.(8) of [39] and p.(3) of [46]). Here, we utilize a differential equation for arbitrary α, β [40] (see App.B.2 for details).

In the "bifurcation approximation", we are at $p \gg \Delta/v_F$, in which region the pairing dynamics dominate. Thus, we can drop the $(\Delta_q/v_F)^2$ term in the denominator, as it only contributes to an infrared cutoff, and instead introduce $(\Delta_0/v_F)^2$ as a lower limit in the integral. Thus, we arrive with a simplified gap equation

$$\Delta_p = \lambda \left(\int_{\Delta_0/v_F}^{p} \frac{dq}{p}\Delta_q + \int_p^{\Lambda} \frac{dq}{q}\Delta_q \right) \tag{3.4}$$

where Λ is an ultraviolet cutoff. We can extend this analysis beyond [41] by now allowing for an arbitrary DOS and an effective Coulomb interaction

$$\Delta(p) = \lambda h_0 \int_0^p k^\beta dk \frac{\Delta_k}{\sqrt{k^2+\Delta_k^2}} \left(\frac{1}{p^\alpha}\right) + \lambda h_0 \int_p^\Lambda k^\beta dk \frac{\Lambda_k}{\sqrt{k^2+\Delta_k^2}} \left(\frac{1}{k^\alpha}\right) \tag{3.5}$$

which is equivalent to the differential equation (see App.B.2)

$$\frac{d^2\Delta(\epsilon)}{d\epsilon^2} + \frac{\alpha+1}{\epsilon}\frac{d\Delta(\epsilon)}{d\epsilon} + g\frac{\alpha\Delta(\epsilon)}{\epsilon^{2+\alpha-\beta}} = 0 \tag{3.6}$$

where $g = g_0/[2^{D-1}\pi^{D/2}\Gamma(D/2)]$, subject to the infrared and ultraviolet boundary conditions, respectively,

$$\left.\frac{d\Delta(\epsilon)}{d\epsilon}\right|_{\epsilon=max[\Delta,\mu]} = 0 \tag{3.7}$$

and

$$\Delta(\epsilon) + \frac{\epsilon}{\alpha}\left.\frac{d\Delta(\epsilon)}{d\epsilon}\right|_{\epsilon=\Lambda} = 0 \tag{3.8}$$

where $J(\Delta)$ is the source function. This yields the solution

$$\Delta(\epsilon) = \Delta\left(\frac{\Delta}{\epsilon}\right)^{\gamma(\epsilon)}\frac{\sin\left[\Phi(\epsilon)+\delta\right]}{\sin\delta} \tag{3.9}$$

where the prefactor is chosen to satisfy the natural normalization condition $\Delta(\epsilon)|_{\epsilon=\Delta} = \Delta$, and the phase of the trigonometric function is given by the expression

$$\Phi(\epsilon) = \sqrt{\alpha g\epsilon^{2r} - \frac{\kappa(\epsilon)}{4}}\left[\frac{1-\left(\frac{\Delta}{\epsilon}\right)^r}{r}\right] \tag{3.10}$$

where $r = (\beta-\alpha)/2$ and the phase shift

$$\delta = \begin{cases} \tan^{-1}\left[\sqrt{4\alpha g\Delta^{2r} - \kappa(\Delta)}/\alpha\right] \ , & \Delta > [\kappa(\Delta)/4\alpha g]^{1/2r} \\ \delta = 0 \ , & \text{otherwise} \end{cases} , \tag{3.11}$$

is determined by the infrared (IR) boundary condition. The slowly varying functions $\gamma(\epsilon)$ and $\kappa(\epsilon)$ are, asymptotically,

$$\gamma(\Delta) = \alpha/2, \qquad \gamma(\Lambda) = (\alpha+\beta)/4 \tag{3.12}$$

and

$$\kappa(\Delta) = \alpha^2 - (\alpha-\beta)^2, \qquad \kappa(\Lambda) = \alpha^2 - \frac{1}{4}(\alpha-\beta)^2. \tag{3.13}$$

The ultraviolet (UV) boundary condition fixes the maximum (zero-momentum) gap in terms of the dimensionless coupling $\tilde{g}$ and upper cutoff Λ:

$$\tan\left[\Phi(\Lambda)\right] + \frac{4}{3\alpha-\beta}\frac{\alpha\tilde{g} - \kappa(\Lambda(\Delta/\Lambda)^r)/4}{\sqrt{\alpha\tilde{g} - \kappa(\Lambda)/4}} = 0, \tag{3.14}$$

where $\tilde{g} = g\Lambda^{2r}$. In the general case $\alpha < \beta$, the UV boundary condition (3.14) yields

$$\Delta \sim \Lambda\left(\tilde{g} - \tilde{g}_c\right)^{1/r} \tag{3.15}$$

for couplings greater than the critical value

$$\tilde{g}_c \approx \frac{1}{16\alpha}\left[(\alpha+\beta)^2 + \pi^2(\beta-\alpha)^2\right] \tag{3.16}$$

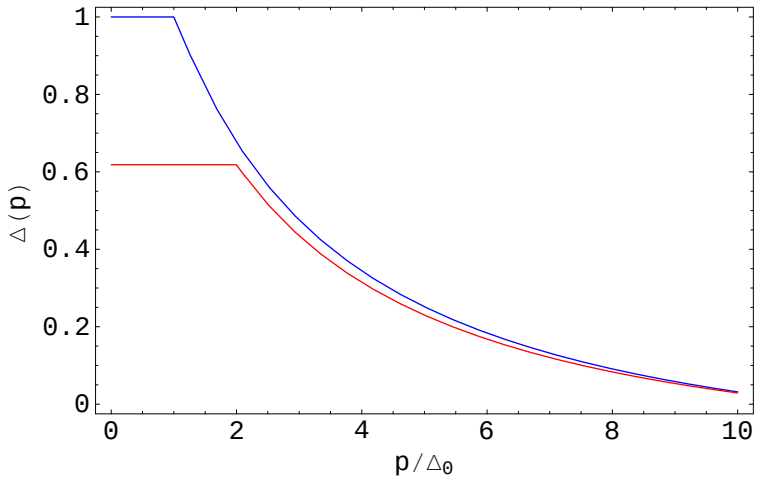

Figure 3.1: Approximate solution to the p-dependent gap equation, $\Delta(p)$ vs. p in units of Δ_0 for $\Delta \geq \mu$ (blue) (eq.3.9) and for $\Delta < \mu$ (red) (eq.3.17). Note that, although the presence of a chemical potential μ suppresses the magnitude of the dynamical gap for lower p-values, the behavior for large $p \gg \max[\Delta, \mu]$ is essentially the same for both.

Technically, the bifurcation approximation is only applicable at relatively high energies and momenta, $\Delta \ll \epsilon$, as noted above. However, as we shall soon see, comparison between the original gap equation (2.22) and this much simpler linearized equation (3.6) shows that this approximate solution actually holds all the way to energies $\epsilon \sim \Delta$.

We may now introduce a finite chemical potential μ, which, depending on the sign, represents a finite density of either particles or holes. As noted earlier, μ provides a cutoff for the momentum integration in the gap equation (2.22), which translates as a point $\epsilon \leq \mu$ at which the solution to the gap equation $\Delta(\epsilon)$ levels off and becomes energy-independent.

Hence, for $\Delta < \mu$, we impose the normalization condition $\Delta(\epsilon)|_{\epsilon=\mu} = \Delta$, thereby arriving at the approximate formula for the counterpart of (3.9)

$$\Delta(\epsilon) = \Delta \left(\frac{\mu}{\epsilon}\right)^{\gamma(\epsilon)} \frac{\sin\left[\Phi(\epsilon) + \delta\right]}{\sin\left[\Phi(\mu) + \delta\right]}. \tag{3.17}$$

Meanwhile, for $\Delta > \mu$, the original solution for $\mu = 0$ (3.9) remains essentially untouched.

In particular, in the marginal case along the line of scale-invariant (or, conformally invariant) scenarios in which $\alpha = \beta$, the general solution to the gap equation for $\mu < \Delta$ (3.9) becomes for $g > g_c = \alpha/4$

$$\Delta(\epsilon) = \Delta \left(\frac{\Delta}{\epsilon}\right)^{\alpha/2} \frac{\sin\left[\sqrt{\alpha g - \alpha^2/4}\ln(\epsilon/\Delta) + \delta\right]}{\sin\delta}, \tag{3.18}$$

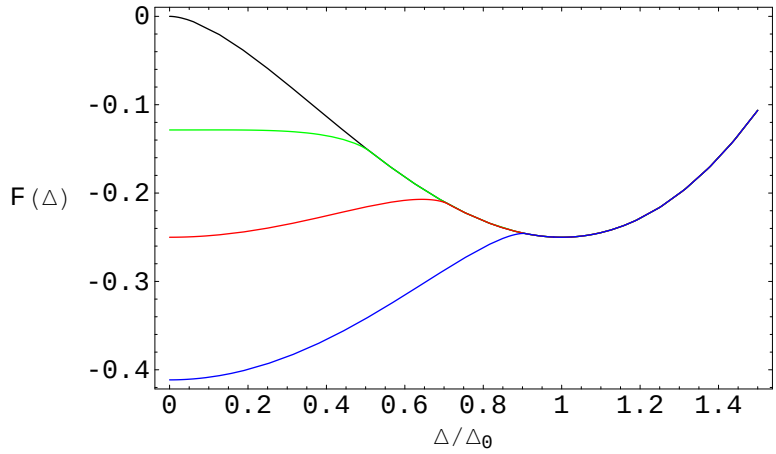

Figure 3.2: Free energy for $\alpha = \beta = 0$ as a function of chemical potential μ (in units of Δ_0): 0 (black), 0.5 (green), $1/\sqrt{2}$ (red), and 1 (blue).

where $\delta = \tan^{-1}\sqrt{4(g/\alpha) - 1}$. Likewise, for $\Delta < \mu$,

$$\Delta(\epsilon) = \Delta\left(\frac{\mu}{\epsilon}\right)^{\alpha/2} \frac{\sin(\sqrt{\alpha g - \alpha^2/4}\ln\epsilon/\Delta + \delta)}{\sin(\sqrt{\alpha g - \alpha^2/4}\ln\mu/\Delta + \delta)}. \tag{3.19}$$

We will use (3.9) and (3.19) throughout the subsequent sections to compute the free energy $F(\Delta, \mu)$ and explore the quantum phase transitions where we see the opening of the gap.

3.2 Quantum Phase Transitions

The conventional method to exploring quantum phase transitions is the Luttinger-Ward approach (see [47, 48, 49, 50] for a very detailed analysis of non-BCS superconducting pairing employing such a technique). However, in the cases we are considering here, application of the Luttinger-Ward or similar methods lead to a badly divergent momentum double integral $\sum_{\mathbf{p},\mathbf{q}} \Delta_p U^{-1}(0, \mathbf{p} - \mathbf{q})\Delta_q$ whose kernel is given by the (generally, highly non-local) inverse operator $U^{-1}(0, \mathbf{p})$. Also, if we are to be able to distinguish global minima from all other extrema (as discussed in the previous section), we would have to compute the $F(\Delta, \mu)$ functional for all Δ, whereas previous analyses simply concerned themselves with computing $F(\Delta_0, \mu)$, i.e., at the global minimum Δ_0 ("condensation energy")[47, 48, 49]. Alternatively, we will employ a technique utilized in the case of highly oriented pyrolytic graphite by Miransky *et al.* (see Ref.[41] and references therein). In this, we will make use of the source function (see App.B.3 for details)

$$J(\Delta) = \left(\Delta(\epsilon) + \frac{\epsilon}{\alpha}\frac{d\Delta(\epsilon)}{d\epsilon}\right)\Big|_{\epsilon=\Lambda} \tag{3.20}$$

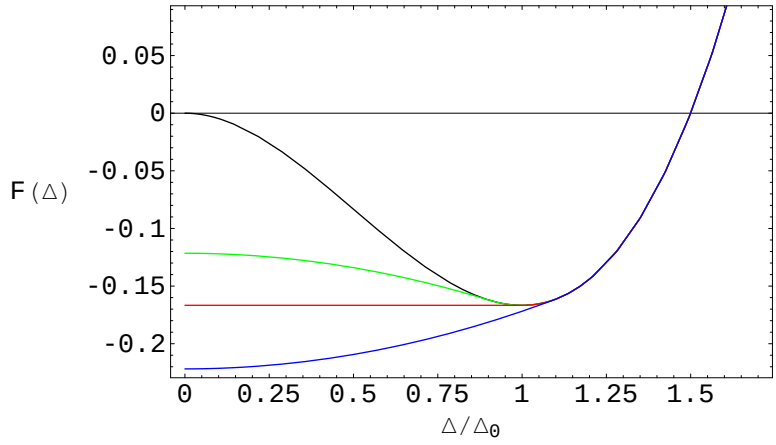

Figure 3.3: Free energy for $\alpha = 0$, $\beta = 1$ as a function of chemical potential μ (in units of Δ_0): 0 (black), 0.9 (green), 1 (red), and 1.1 (blue).

and the order parameter

$$\sigma(\Delta) = Tr[\hat{\tau}_1 \int \frac{d\omega}{2\pi} \sum_{\mathbf{q}} \hat{G}(\omega, \mathbf{q})] = -\left. \frac{\epsilon^{\alpha+1}}{\alpha g_0} \frac{d\Delta(\epsilon)}{d\epsilon} \right|_{\epsilon=\Lambda} \tag{3.21}$$

which together will determine the (regularized) effective potential

$$F(\Delta, \mu) = \int_0^{\Delta} d\Delta' \frac{d\sigma(\Delta')}{d\Delta'} J(\Delta') + F(0, \mu). \tag{3.22}$$

The integration constant $F(0, \mu)$ is to be found from the equation for the density of excess particles

$$-\frac{\partial F(\Delta, \mu)}{\partial \mu} = n(\mu) = \sum_{\mathbf{p}, \mp} \theta(\mu \mp E_p). \tag{3.23}$$

We now turn to specific examples.

3.2.1 $\alpha = \beta = 0$: BCS

We start with the standard BCS pairing between fermions, characterized by a short-ranged potential and a finite DOS.

In this case, for $\mu < \Delta$ the gap equation (2.22) yields the standard result $\Delta(\epsilon) = \Delta_0 = \Lambda e^{-1/g}$. From this, the free energy

$$F_>(\Delta, \mu) = \frac{g\Delta^2}{4g_0} \left(\frac{1}{g} - \frac{1}{2} - \ln \frac{\Lambda}{\Delta} \right), \tag{3.24}$$

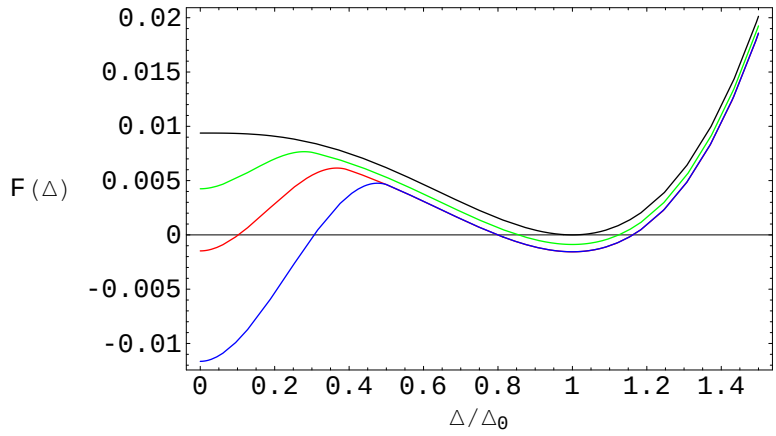

Figure 3.4: Free energy for $\alpha = \beta = 1$ as a function of chemical potential μ (in units of Δ_0): 0 (black), 0.4 (green), 0.6 (red), and 0.8 (blue).

whereas for $\Delta < \mu$ we obtain

$$F_<(\Delta,\mu) = \frac{g\Delta^2}{4g_0}\left(\frac{1}{g} - \frac{1}{2} - \ln\frac{\Lambda}{\mu + \sqrt{\mu^2 - \Delta^2}}\right) - \frac{g}{2g_0}\mu\sqrt{\mu^2 - \Delta^2}, \tag{3.25}$$

the last term being proportional to the particle density $n = \frac{1}{2}\sqrt{\mu^2 - \Delta^2}$. Plotting $F(\Delta)$ vs. Δ for various values of μ (fig.3.2), we see that, as μ approaches the critical $\mu_c = 1/\sqrt{2}$, a secondary "dip" develops at $\Delta = 0$ but the global minimum remains at $\Delta = \Delta_0$.

Finally, at $\mu = \mu_c = (1/\sqrt{2})\Delta_0$, there is a degeneracy in ground states, and as μ increases further past μ_c, the global minimum jumps *discontinuously* to $\Delta = 0$ – suggesting a *first*-order phase transition – and the order parameter vanishes. This is consistent with the known superconducting BCS transition in the presence of an external magnetic field.

3.2.2 $\alpha = 0$, $\beta = 1$: short-ranged potential and a linear density of states $\nu(\epsilon) \propto \epsilon$

As another example, we can also consider the limiting case ($\alpha \to 0$) in which we have a short-range potential but now have a *linear* DOS – indicative of Dirac particles – thus stepping outside of the Fermi-liquid realm. Because $\alpha = 0$, we find that the gap function takes on a particularly simple form: $\Delta(\epsilon) \to \Delta_0 = g_c^{-1} - g^{-1}$ for $\mu < \Delta$. In this case, the free energy

$$F(\Delta,\mu) = \begin{cases} \frac{g}{2g_0}\Delta^2\left(\frac{1}{3}\Delta - \frac{1}{2}\Delta_0\right), & \mu < \Delta \\ \frac{g}{2g_0}\left(-\frac{1}{6}\mu^3 + \frac{1}{2}\mu\Delta^2 - \frac{1}{2}\Delta_0\Delta^2\right), & \Delta < \mu \end{cases} \tag{3.26}$$

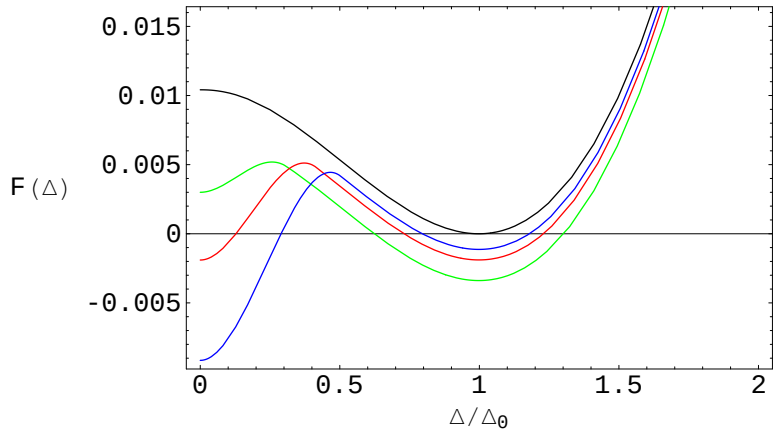

Figure 3.5: Free energy for $\alpha = 1/2$, $\beta = 1$ as a function of chemical potential μ (in units of Δ_0): 0 (black), 0.5 (green), 0.7 (red), and 0.8 (blue).

where, in the latter scenario the free energy incorporates an excess electron density $n(\mu) = \frac{1}{2}(\mu^2 - \Delta^2)$.

The minimum of the free energy exists for all $g > g_c = 1/\Lambda$. In contrast to the BCS scenario, note from Fig.3.3 that $F(\Delta)$ becomes *independent* of $\Delta(\epsilon)$ right at $\mu_c = \Delta_0$, which suggests that we may have a *continuous* phase transition. However, it is possible that if fluctuations about the mean-field solution were taken into account, the transition would be of first order, albeit weakly.

3.2.3 $\alpha = \beta = 1$: long-ranged interactions and linear density of states $\nu(\epsilon) \propto \epsilon$

While our previous two examples provide some specific (limiting) examples, our main motivation is in *long*-ranged, i.e., unscreened, Coulomb interactions. Having a linear density of states, as before, $\xi_p \propto p \Rightarrow \nu(\epsilon) \propto \epsilon \Rightarrow \beta = 1$, we now also have unscreened Coulomb interactions $U^{(0)}(\mathbf{q}) = g/q \Rightarrow \alpha = 1$. In contrast to the two previous examples, the gap is now non-trivial, and which also has the aforementioned momentum scale-invariance. The solution to the gap equation (3.18) (see App.C.1 for details)

$$\Delta(p) = \frac{\Delta}{\sin\sqrt{4g-1}}\sqrt{\frac{\Delta}{p}}\sin\left[\sqrt{g-1/4}\ln\frac{p}{\Delta} + \sqrt{4g-1}\right] \tag{3.27}$$

for $\mu \leq \Delta$, and

$$\Delta(p,\mu) = \frac{\Delta}{\sin\left[\sqrt{g-1/4}\ln\frac{\mu}{\Delta} + \sqrt{4g-1}\right]}\sqrt{\frac{\mu}{p}}\sin\left[\sqrt{g-1/4}\ln\frac{p}{\Delta} + \sqrt{4g-1}\right] \tag{3.28}$$

for $\mu > \Delta$, which is the same as that obtained by Refs [39, 46, 41, 51]. In this case, the UV boundary condition (3.14) yields

$$\Delta = \Lambda \exp\left(-\frac{2\pi - 4\delta}{\sqrt{4\alpha(g - g_c)}}\right). \tag{3.29}$$

From that, the free energy for $\Delta < \mu$

$$F(\Delta, \mu) = \frac{g}{2g_0}\left[I_<(\Delta, \mu) - I_<(\Delta_0, \mu) - \frac{1}{2}\int_\Delta^\mu d\omega(\omega^2 - \Delta^2)\right] \tag{3.30}$$

where

$$I_<(\Delta, \mu) = \mu \int_0^\mu d\omega\omega \frac{\ln(\Delta_0/\omega)[5 - \ln(\Delta_0/\omega)]}{(2 + \ln \mu/\omega)^2} \tag{3.31}$$

whereas for $\Delta > \mu$

$$F_>(\Delta, \mu) = \frac{g}{2g_0}\left[I_>(\Delta, \mu) - I_>(\mu, \mu) + I_<(\mu, \mu) - I_<(\Delta_0, \mu)\right] \tag{3.32}$$

where

$$I_>(\Delta, \mu) = -\frac{2}{3}\Delta^3 - 2\Delta^3 \ln\frac{\Delta_0}{\Delta} + \frac{\Delta^3}{2}\ln^2\frac{\Delta_0}{\Delta}. \tag{3.33}$$

There are several phenomena to make note of here. First: from Fig.3.4, we see that there is a local maximum at $\Delta = \Delta_0 e^{-14/3}$ for $\mu = 0$, which gradually moves to the right as μ increases. Second: there is global maximum located at Δ_0, which first moves down slightly as μ increases, but otherwise stays close to its initial position up to $\mu_c \approx 0.6\Delta_0$. Third, note that the free energy's behavior as $\mu \to \mu_c$ suggests a first order phase transition.

These results vary markedly from conclusions reached previously by other groups [52, 53, 54, 41, 51]. In Refs[52, 53, 54], it was conjectured that for $\mu = 0$, the corresponding transition is of **infinite** order. Also, Refs[41, 51] found a very different value for the critical chemical potential, $\mu_c = \Delta_0/\sqrt{2}$. However, this result arises because the authors in [41, 51] introduced the chemical potential as a lower limit in the integration over ξ_p rather than E_p, which becomes inaccurate for $\mu \sim \Delta_0$.

Moving to more general dispersion relations parameterized by μ but maintaining a linear DOS, we find that the critical chemical potential $\mu_c = -0.04\eta^2 + 0.22\eta + 0.21$ for $\alpha = \beta = 1$. (See App.C.1.2 for details.)

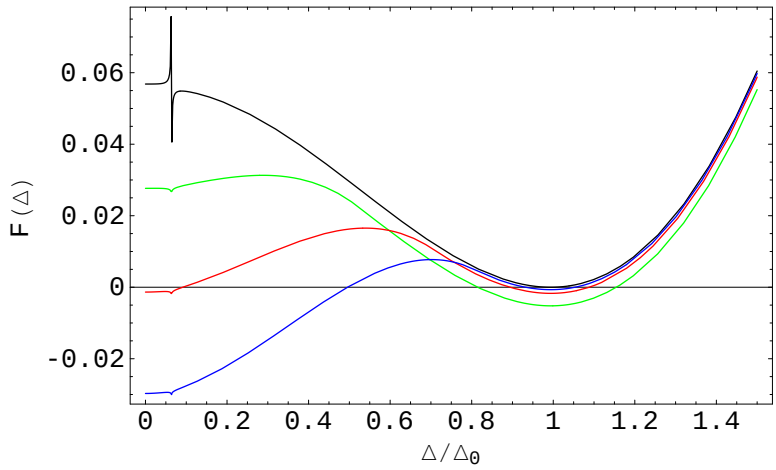

Figure 3.6: Free energy for $\alpha = 2/3$, $\beta = 1$, and $\eta = 1$ as a function of chemical potential μ (in units of Δ_0): 0 (black), 1/2 (green), 0.69 (red), and 0.8 (blue).

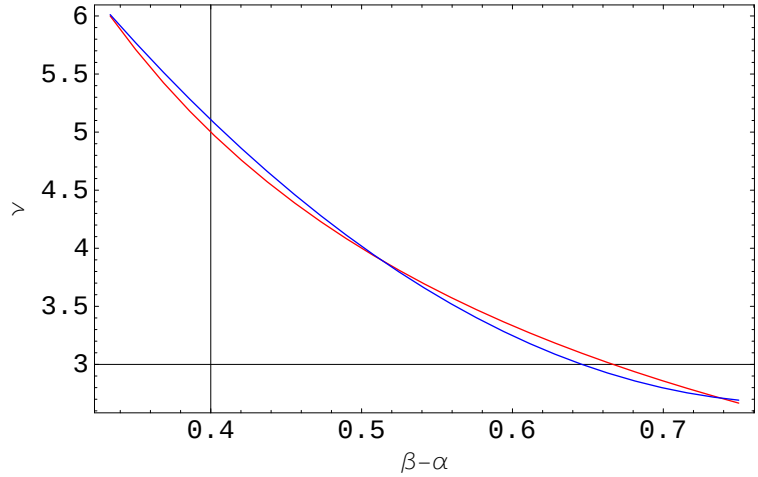

Figure 3.7: Exponent ν in the maximum gap $\Delta_0 \propto (\tilde{g} - \tilde{g}_c)^\nu$ as a function of $\beta - \alpha$ (blue) vs. the expected exponent $1/(\beta - \alpha)$ (red).

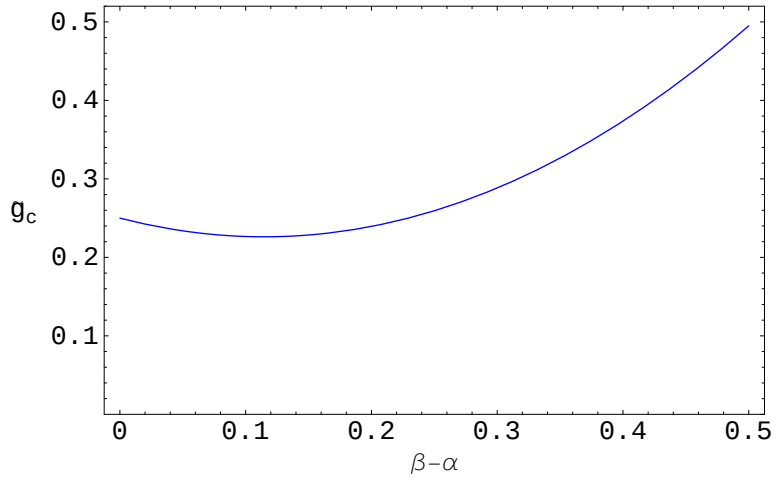

Figure 3.8: Critical coupling $\tilde{g}_c$ as a function of $\beta - \alpha$.

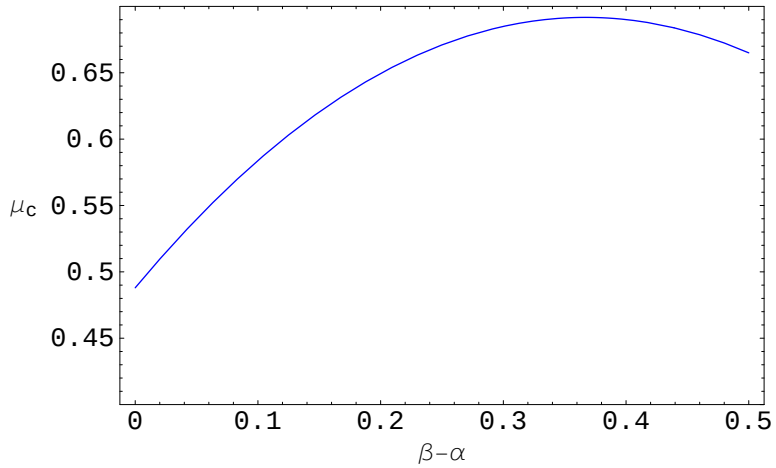

Figure 3.9: Critical value of the chemical potential μ_c (in units of Δ_0) as a function of $\beta - \alpha$.

3.2.4 $\alpha = 1/2,\ \beta = 1$

As a last example, we move away from the conformally (scale) invariant line $\alpha = \beta$ and into the lower wedge $\alpha < \beta$. Although we pick $\alpha = 1/2$, all of the results will apply for all $1/3 < \alpha < 1$. ($\beta = 1$, as we are continuing to consider Dirac-like particles with linear DOS and energy dispersion.) Physically, $\alpha = 1/2$ corresponds to the scenario of Coulomb interacting electrons in an infinite stack of graphene layers, with an interaction $U^{(0)}(\mathbf{q}) = g_0/\sqrt{q}$. A subtlety is that now we are dealing with a *non*-conformally invariant system; therefore the coupling g will be momentum-dependent and the free energy will become g-dependent [4, 7, 8, 9, 10, 11, 12, 3, 39, 55, 46]. For details, see App.C.2.

Note that, essentially, the free energy behaves much the same as in the conformally invariant case $\alpha = \beta$, indicating a first-order phase transition at $\mu_c \approx 0.7\Delta_0$. Fitting the plot of μ_c vs. η, we find that $\mu_c = -0.03\eta^2 + 0.201\eta + 0.2375$.

As mentioned, a similar phenomenon happens for all $\beta/3 < \alpha < \beta$. As an example, consider $\alpha = 2/3,\ \beta = 1$. (See App.C.3 for details.) In this case, the free energy functional for various μ is given in fig.3.6. (The detail at $\Delta \sim 0.6$ is a mathematical artifact.) Here, too, we see a very similar quantum phase transition, also indicative of being first-order, occurring at $\mu = \mu_c \approx 0.69\Delta_0$.

3.3 Critical Phenomena

In all of the above analysis, it was never assumed that the maximum gap $\Delta_0 \sim \Lambda\,(\tilde{g} - \tilde{g}_c)^{\frac{2}{\beta-\alpha}}$, as expected. In these actual worked-out examples, does this power-law relation hold true?

To find out, we fit a curve to the calculated $\Delta_0 \propto (\tilde{g} - \tilde{g}_c)^{\nu}$ for each different $\alpha,\ \beta$ scenario and compare the power-law exponent. The fitted curve yields a power-law relation that is very close to the expected curve $1/(\beta - \alpha)$ (fig.3.7).

Likewise, we can examine the power-law relationship of the critical coupling g_c itself on $\beta - \alpha$. From the above values of g_c and $\beta - \alpha$, we find a fitting function $g_c \sim 1.81(\beta - \alpha)^2 - 0.415(\beta - \alpha) + 0.25$, the plot of which we see in fig.3.8. This result does reflect what we expect to see, eq.(3.16), above.

If we try repeating the procedure for μ_c vs. $\beta - \alpha$, we find a fitting function $\mu_c \sim -1.512(\beta - \alpha)^2 + 1.11(\beta - \alpha) + 0.488$, the plot of which we see in fig.3.9. Such results are less conclusive.

3.4 Phase Transitions and Strongly Correlated Systems

Systems with shorter-ranged interactions (lower values of α) and/or stronger DOS suppression (higher values of β) bear a stronger propensity towards excitonic pairing. Furthermore, the excitonic order emerges at sufficiently strong repulsive couplings and survives up to a finite critical doping by excess carriers.

The above results for the BCS transition are also consistent in describing the onset of an excitonic instability in the case of Fermi liquids with screened repulsive interactions. However, a more accurate picture of such, in which case the transition is driven by a variable density in which the number of carriers is not fixed, would indicate a *second*-order transition instead of first.

An important lesson of this analysis is that it is not adequate to evaluate $F(\Delta, \mu)$ only at its extrema. If we had done so above, we might not have been able to distinguish local from global extrema, or even worse yet, from maxima. Due to previous work by [29, 30], there has been great confusion over results purporting to show that a nontrivial solution exists for $\mu > \Delta_0/2$, which was later used to suggest that an excitonic state exists in hexaborides [31, 32, 33, 34, 35, 36] – something which is considered to be unlikely in hexaborides from an experimental point of view [37]. However, from our own analysis in fig.3.2, we see that the claimed point was a local *maximum*, not a minimum, and furthermore that such a transition cannot take place for this range of μ, consistent with experimental findings.

In the long-ranged Dirac case, $\alpha = \beta = 1$, the UV boundary condition (3.29) is reminiscent of the Kosterlitz-Thouless (KT) transition in XY-symmetrical 2D systems. Furthermore, similar behavior has been found in the context of 3D relativistic chiral symmetry breaking, in which case this transition signaled the onset of a conformally invariant critical regime [52, 53, 54]. Given that the above results have appeared in *non*-relativistic systems, and instead appear to arise from momentum scale-invariance, suggest that (3.29) does not arise from the Lorentz-invariance of such systems, but instead from the scale invariance of the underlying "radial" gap equation.

Future experimental work will be needed to determine the status of the quantum phase transitions presented here, particularly in comparison to alternate predictions, such as the Stoner instability resulting in a fully polarized ferromagnetic state, or the development of c-axis antiferromagnetism [56, 57, 58, 59, 60].

There remains a great need for comprehensive analysis of non-BCS pairing scenarios with long-range interactions in nonmetallic systems. In particular, the customary practice for analyzing such systems has been to replace the unscreened Coulomb interaction with the Hubbard-like onsite repulsion – the only apparent motivation for which being greater ease in numerical simulations. How *accurate* such a practice is in accurately describing the physics of nonmetallic systems is not clear. However, our observed differences in the behavior at zero and finite α should serve as a warning against replacing genuinely long-ranged interactions with short-ranged ones.

Chapter 4

Disorder in Nodal Fermion Systems

So far, we have been focusing on relatively strong effects of Coulomb correlations. More subtle effects may exist which may not be strong enough to develop a spectral gap, but are nonetheless significant enough to cause noticeable experimental effects. Such effects may not be revealed in two-particle response functions, such as longitudinal and Hall DC conductivities. As measurements on conventional 2D electron gases (2DEG) suggest, two-particle response functions are only weakly affected by correlations due to the particle-particle interactions because of cancellations between the self-energies and vertex corrections, which themselves can be formidable. Thus, we seek possible reflections of interacting Dirac particles in single-particle probes [56]. In particular, we focus on the so-called "zero-bias" anomaly [61, 62].

The zero-bias anomaly refers to a phenomenon universal to both metals and semiconductors in any dimension, in which electron-electron interactions in the presence of disorder result in a negative correction to the local tunneling density of electron states, which is singular at the Fermi energy. This leads to a suppression of the tunneling single-particle DOS at the Fermi surface, reflected in the conductance of a point tunnel contact [63]. This anomaly was first discussed in terms of short-ranged diffusive systems by Altshuler and Aronov [64, 65], later extended to long-ranged Coulomb interactions [66]. More recently, this analysis has been extended to 2D electron layers at ballistic energies ($\epsilon > 1/\tau$, where τ is the relaxation time) [67, 68, 69].

In previous discussions in the context of tunneling measurements, others have primarily focused on strong disorder [70, 71, 72]. In so doing, however, observed effects are not universal and are more likely to reflect on the impurity potential of the system in question than on the

Coulomb correlations themselves. Such studies find the near-impurity DOS to be very similar to that obtained in the case of a d-wave superconductor, in which the Coulomb interactions are completely screened by the condensate [73].

To avoid this pitfall, we consider particularly weak disorder – close to the clean limit. By varying the coupling strength of the Coulomb interaction, the quasiparticle width γ, and the biasing voltage V, we should be able to see more clearly what effects there may be on interacting Dirac particles.

Dirac physics is best revealed in the ballistic regime, whereas the diffusive regime renders results deceptively similar to that of conventional 2DEG [56]. This phenomenon is evident not only in theory, but also experimentally as well. The electric field effect in few-layer graphite [21] is observed at which the electronic transport is ballistic at submicrometer distances.

Recall from chapter 2 the Hamiltonian

$$\begin{aligned} H = iv_F \sum_{\alpha=1,2} \int_{\mathbf{r}} \Psi_\alpha^\dagger \left[\hat{\tau}_x \nabla_x + (-1)^\alpha \hat{\tau}_y \nabla_y \right] \Psi_\alpha \\ + \frac{v_F}{4\pi} \sum_{\alpha,\beta=1,2} \int_{\mathbf{r}} \int_{\mathbf{r}'} \Psi_\alpha^\dagger (\mathbf{r}') \Psi_\alpha (\mathbf{r}') \frac{g}{|\mathbf{r} - \mathbf{r}'|} \Psi_\beta^\dagger (\mathbf{r}) \Psi_\beta (\mathbf{r}) \end{aligned} \tag{4.1}$$

where, as before, the bare coupling constant $g_0 = 2\pi e^2/\epsilon_0 v_F \approx 2 - 3$ and v_F is the Fermi velocity.

The pseudospinor wavefunctions Ψ_α are composed of spin-1/2 electron wavefunctions on the A and B sublattices of the bipartite hexagonal lattice of graphene. The triplet of Pauli matrices $\hat{\tau}_i$ acts in the space of the Ψ_α. We are now no longer assuming the instantaneous exchange approximation as we did in deriving the gap equation in previous chapters.

The (retarded) Coulomb interaction

$$U^R (\omega, \mathbf{q}) = \frac{(g_0/q)}{1 + (g_0/q)\, \Pi^R (\omega, \mathbf{q})}. \tag{4.2}$$

The combined effect of this and disorder interactions on the fermionic propagator is encoded in the self-energy and polarization.

The quasiparticle propagator in the presence of disorder is

$$\hat{G}_\alpha^R (\omega, \mathbf{p})^{-1} = (\omega + \mu)\, \hat{\mathbf{1}} - v_F \left[\hat{\sigma}_x p_x + (-1)^\alpha \hat{\sigma}_y p_y \right] + \hat{\Sigma}^R (\omega, \mathbf{p}) \tag{4.3}$$

where the fermion self-energy

$$\hat{\Sigma}^R(\omega,\mathbf{p}) = \int \frac{d\omega}{(2\pi)} \sum_{\mathbf{q}} \Big[ImU^A(\omega,\mathbf{q})\, \hat{G}^R(\epsilon+\omega,\mathbf{p}+\mathbf{q}) \coth\frac{\omega}{2T} - U^A(\omega,\mathbf{q})\, Im\hat{G}^R(\epsilon+\omega,\mathbf{p}+\mathbf{q}) \tanh\frac{\epsilon+\omega}{2T} \Big] \Gamma(\omega,\mathbf{q}), \tag{4.4}$$

Π is the polarization operator, and Γ the vertex correction.

The polarization at $T=0$ and no disorder is given by the purely imaginary ($Re\Pi = 0$ for $T=0$)

$$\Pi(\omega,\mathbf{q}) = \frac{q^2}{\sqrt{q^2-(\omega+i\gamma)^2}-\gamma}$$

whereas in the presence of disorder, $q,\omega < \gamma$,

$$\Pi(\omega,\mathbf{q}) = \nu \frac{Dq^2}{Dq^2 - i\omega}$$

where $D = \frac{v_F^2}{2\gamma}$ and v_F is the Fermi velocity. If $T \neq 0$,

$$Im\Pi(\omega,q) = \frac{\omega}{T}\frac{q^2}{\sqrt{q^2-\omega^2}}\mathcal{O}(\omega-q) \tag{4.5}$$

$$Re\Pi(\omega,q) \cong T\ln 2 + \mathcal{O}\left(q^2\omega^2/T\right) \tag{4.6}$$

The coupling in the interaction is not constant, but varies in strength with the frequency ω.

The subsequent renormalization group (RG) equation [10, 11, 12, 3, 9, 13]:

$$\frac{dg(\omega)}{d\ln(\Lambda/\omega)} = -\frac{1}{8\pi}g^2(\omega) \tag{4.7}$$

the approximate solution of which being

$$g(\omega) \approx g_0/[1+(g_0/8\pi)\ln(\Lambda/\omega)] \tag{4.8}$$

where Λ is an upper cutoff of order the electronic bandwidth. The RG flow terminates below the energy scale $\sim \max[T,\mu,\gamma]$ [56].

4.1 Density of States

We may now calculate the DOS for variable g_0,γ,T,D and ϵ. The DOS for the non-interacting system at the Fermi energy is given by the bare loop

$$\nu_0 = -\frac{1}{\pi} ImTr \sum_{\mathbf{p}} \hat{G}_0^R(0,\mathbf{p}) \approx max\left[\frac{\gamma}{2\pi v_F^2}\ln\frac{\Lambda}{\gamma}, \frac{4\mu}{v_F^2\pi}\right], \tag{4.9}$$

where $\hat{G}_0^R(0,\mathbf{p})$ is the bare propagator, which includes impurity-induced broadening but not inelastic scattering. As we include interactions, the first interaction corrections to the bulk DOS are

$$\delta\nu(\epsilon) = \frac{1}{\pi}\sum_{\mathbf{p}} ImTr\left[\hat{G}_0^R(0,\mathbf{p})\right]^2 \tilde{\Sigma}(\epsilon,\mathbf{p}) \propto \begin{cases} -g\epsilon \ln\frac{\Lambda}{\epsilon}, & \epsilon, T > \gamma \\ -\frac{\nu_0}{\sigma_0}\ln\frac{\gamma}{\epsilon}\ln\frac{\tilde{\gamma}}{\epsilon}, & \epsilon, T < \gamma \end{cases} \tag{4.10}$$

where $\tilde{\gamma} = \gamma\sigma_0^4 g_\gamma^4$. In the ballistic regime, this will include an additional logarithmic factor due to a kinematic "light-cone" singularity.

Given the strength of the bare Coulomb interaction, it is conceivable that higher order corrections to the DOS may be quite significant in modifying the behavior of Dirac fermions systems. Thus, we turn to nonperturbative techniques to probe further.

4.2 The "tunneling action" approach

Applying the methods of [74, 61, 62, 75, 76] to graphene [56], we obtain a tunneling DOS

$$\nu(\epsilon) \approx -\frac{1}{\pi} ImTr \int_{-\infty}^{\infty} dt \hat{G}_0^R(\mathbf{0},t)\, e^{-S(t)+i\epsilon t}. \tag{4.11}$$

In this, the disorder-averaged Green function for the Dirac fermions $G_0^R(\mathbf{0},t) \propto \frac{e^{-\gamma t}}{t^2}$ includes the disorder-induced self-energy but not the Coulomb interactions between the Dirac fermions. These are incorporated into (4.11) through the imaginary part of the action (the real portion will only contribute to the overall renormalization).

$$S(t) = \int_0^\Lambda \frac{d\omega}{4\pi}\sum_{\mathbf{q}} ImU(\omega,\mathbf{q}) \coth\frac{\omega}{2T}\int_0^t dt_1 \int_0^t dt_2 e^{-i\omega(t_1-t_2)}\left\langle e^{i\mathbf{q}(\mathbf{r}(t_1)-\mathbf{r}(t_2))}\right\rangle \tag{4.12}$$

where $S(t)$ is the action for moving a charge in the target substrate as a new electron tunnels in. This describes, for example, the spreading of excess charge due to tunneling from a STM tip into a graphene sample [56, 69].

Extending to experimental measurements, we may calculate the DOS in terms of the conductance, $G(V)$. The conductance, which is measured by tunneling from one substance to another, is given by

$$G(V) = \frac{dI}{dV} \tag{4.13}$$

where the current $I(V)$ is measured by the convolution

$$\propto \frac{d}{dV}\int_0^V \nu_0(\epsilon)\,\nu(V-\epsilon)\,d\epsilon, \tag{4.14}$$

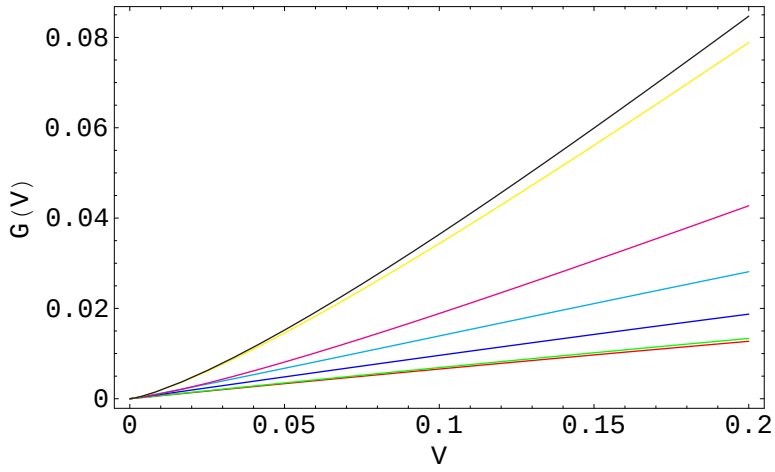

Figure 4.1: $G(V)$ vs. V: $g_0 = 1/100$ (red), $g_0 = 1/10$ (green), $g_0 = 1$ (blue), $g_0 = 3$ (cyan), $g_0 = 10$ (magenta), $g_0 = 100$ (yellow), $g_0 = 1000 \sim \infty$ (black).

$\nu_0(\epsilon)$ being the DOS for the first substance and $\nu(\epsilon)$ is that of the second. Thus, the conductance is given in terms of the Fourier transform of the Green's functions $\mathcal{G}_0(\mathbf{0}, t)$ and $\mathcal{G}(\mathbf{0}, t)$

$$G(V) \propto \frac{d}{dV} \int_0^\infty \mathcal{G}^R(\mathbf{0}, t)\, \mathcal{G}_0^R(\mathbf{0}, t)\, e^{iVt} dt \tag{4.15}$$

The Green's function $\mathcal{G}_0^R(\mathbf{0}, t) \sim 1/t$, and that of the linear Dirac fermions is the same as that given previously. Putting all of this together, we may write

$$G(V) \propto Im\ i \int_0^\infty \frac{dt}{t^2} e^{iVt} e^{-S(t)}. \tag{4.16}$$

In the large bias regime, we may ignore γ entirely, and (4.12) becomes

$$S(t) \approx \begin{cases} \frac{g_0^2}{(4\pi)^2} \ln(\Lambda t), & g_0 \ll 1 \\ \frac{1}{\pi^2} \ln(\Lambda t) \ln\left[\frac{8\pi e}{\ln(\Lambda t)}\right], & g_0 \gg 1 \end{cases} \tag{4.17}$$

for weak and strong couplings, respectively [56].

In general,

$$\begin{aligned} S(V > T, \gamma) &= \int_{1/t}^{\Lambda} \frac{d\omega}{\omega^2} \int d^2q \frac{g_\omega^2 \sqrt{\omega^2 - q^2}}{(\omega^2 - q^2) + g_\omega^2 q^2} \\ &= \int_{1/t}^{\Lambda} \frac{d\omega}{\omega} g_\omega^2 \int_0^1 dx \frac{\sqrt{1-x}}{1 - x + g_\omega^2 x} \end{aligned} \tag{4.18}$$

where the coupling

$$g_\omega = \frac{g_0}{1 + \frac{g_0}{4} \ln \frac{\Lambda}{\omega}}. \tag{4.19}$$

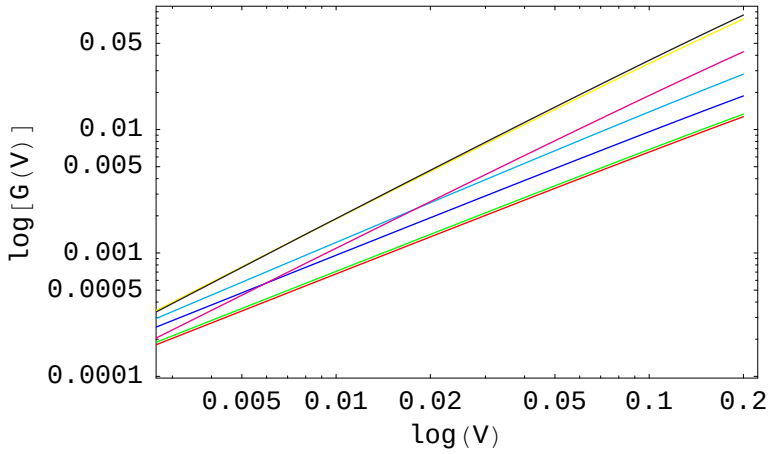

Figure 4.2: $\ln[G(V)]$ *vs.* $\ln V$: The couplings with their respective (approximate) anomalous exponents are $g_0 = 1/100$ (red), $\eta \approx 0$; $g_0 = 1/10$ (green), $\eta \approx 0$; $g_0 = 1$ (blue), $\eta \ll 0.5$; $g_0 = 3$ (cyan), $\eta \approx 0.05$; $g_0 = 10$ (magenta), $\eta \approx 0.24$; $g_0 = 100$ (yellow), $\eta \approx 0.25$; $g_0 = 1000 \sim \infty$ (black), $\eta \approx 0.3$.

From (4.16), we obtain the conductance $G(V)$ for various bare couplings g_0 (see fig.4.1) – see App.D for details. The conductance curves $G(V)$ for various couplings g_0 is given in fig.4.1.

To more clearly see the power-law relation of $G(V)$ on V, we generate a log-log plot of these results (fig.4.2). From fig.4.2, we see that $G(V)$ evolves from being a purely algebraic function of V at small couplings ($g_0 < 1$) to a more complicated relation, $G(V) \propto V^{1+\eta}$ at moderate to large g_0, the power-law given by the slope. The anomalous exponent η, which characterizes the zero-bias anomaly, increases monotonically. It has been predicted [56] that $\eta = g_0^2/(4\pi)^2$ for weak coupling, whereas asymptotically for large couplings, $\eta = (1/\pi^2)\ln 8\pi e \approx 0.43$. From these explicit calculations, what we see reflects this trend quite well.

For weak coupling, we find that the Fourier transform is very close to a power law relation.

$$G(V) \sim V \cdot e^{-S(t\sim 1/V)} \tag{4.20}$$

$$\sim V^{1+\eta} = V(1 + \eta \ln V + ...) \tag{4.21}$$

in which the last term contains a logarithmic correction seen in the correction to the DOS

$$\nu(\epsilon) = \epsilon + g^2 \epsilon \ln \epsilon + ... \tag{4.22}$$

What we obtain is quite similar to the experimental results obtained by West *et al.* [77] in 2-D lateral tunnel junctions and biases $-7.2 \leq V \leq 7.2$. Our results also agree well with the

experimental findings by Kim *et al.* [18] in graphitic samples of varying thickness. Currently, this is still a work in progress, to be published at a later time. It would be interesting to extend the above analysis to samples of varying thickness as well, to explore the transition from bulk to effectively planar systems.

Chapter 5

Applications and Repercussions

In concluding this thesis, we now turn to repercussions on other physically different nodal fermion systems. As mentioned in chapter 1, there exist other systems that also contain Fermi points. Despite being of very different physical origin from graphene, universal symmetries due to their formal similarities may allow us to make significant conclusions concerning these other systems as well.

5.1 Spontaneous Chiral Symmetry Breaking

In recent years, many condensed matter theorists have come to portray certain phase transitions in some systems as examples of spontaneous chiral symmetry breaking (CSB), long explored in the context of high energy particle physics. I point out the formal relation of these scenarios to those that I have discussed above to demonstrate how the quantum phase transitions explored above carry over to these systems as well. To introduce this topic, we take a step back and discuss CSB in the context of layered graphite [39, 55].

Again, we return to the Hamiltonian from previous chapters, written in terms of four-component Dirac spinors:

$$H_0 = iv_F \sum_{\sigma=1}^{N} \int_{\mathbf{r}} \bar{\Psi}_\sigma \left[\hat{\gamma}_1 \nabla_x + \hat{\gamma}_2 \nabla_y\right] \Psi_\sigma \tag{5.1}$$

$$H_C = \frac{v_F}{4\pi} \sum_{\sigma,\beta=1}^{N} \int_{\mathbf{r}} \int_{\mathbf{r}'} \bar{\Psi}_\sigma \left(\mathbf{r}'\right) \Psi_\sigma \left(\mathbf{r}'\right) \frac{g}{|\mathbf{r} - \mathbf{r}'|} \bar{\Psi}_\beta \left(\mathbf{r}\right) \Psi_\beta \left(\mathbf{r}\right) \tag{5.2}$$

The Dirac spinors $\Psi_\sigma = (\psi_{1\sigma}, \psi_{2\sigma})$ can be used to form chiral fermions $\Psi_{L,R\sigma} = \frac{1}{2}\left(\mathbf{1} \pm \hat{\gamma}_5\right) \Psi_\sigma$, where $\hat{\gamma}_5 = \mathbf{1} \otimes \tau_2$ anticommutes with all $\hat{\gamma}_\mu$ and τ_i denote Pauli matrices.

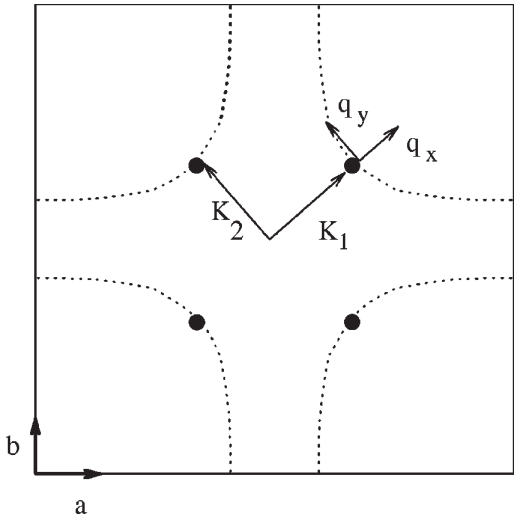

Figure 5.1: d-wave Brillouin zone, with nodes [5].

Although the Coulomb interaction term H_C violates Lorentz invariance, it *does* remain invariant under $U(2N)$ rotations of the $2N$-component vector $(\Psi_{L\sigma}, \Psi_{R\sigma})$. (The free particle portion H_0 is invariant under both Lorentz transformations and $U(2N)$ rotations.) This *chiral invariance* of the complete Hamiltonian allows for the possibility of spontaneous chiral symmetry breaking, manifested in the appearance of a fermion mass (corresponding to an order parameter), breaking this continuous chiral symmetry $U(2N) \to U(N) \otimes U(N)$. (See App.A.) (2+1)-D CSB can be formulated in terms of two distinct interactions: interactions with a bosonic scalar (Higgs-Yukawa) and interactions with a gauge field (QED_3).

5.1.1 Effective Higgs-Yukawa Interactions in Condensed Matter Systems

In terms of Higgs-Yukawa (HY) interactions, CSB is brought about through interactions with some HY bosonic mode, which couples to the Dirac fermions via the mass operator $\sum_\sigma \bar{\Psi}_\sigma \Psi_\sigma$. This transition occurs for all N, where N equals the number of fermion species, as long as the HY coupling $g_{HY} \geq g_c$. In such a scenario, the Dirac fermions couple to a real boson field ϕ, itself governed by a generic ϕ^4 theory [78]:

$$\mathcal{L}_\phi = \frac{1}{2}\left[\frac{1}{c^2}\left(\partial_0\phi\right)^2 - \left(\nabla\phi\right)^2 - m^2\phi^2\right] - \frac{\lambda}{24}\phi^4. \tag{5.3}$$

ϕ corresponds to the imaginary part of the total gap function.

This was invoked in suggesting the possibility of a second pairing transition in planar d-wave superconductors, $d \to s^* + id$ or $d \to d_{x^2-y^2} + id_{xy}$, at a quantum-critical point lying

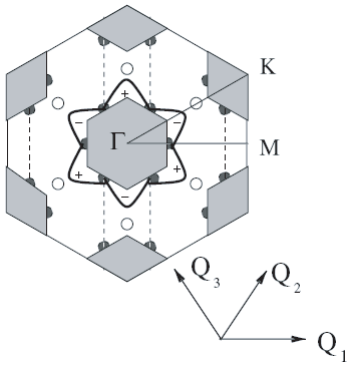

Figure 5.2: f-wave Brillouin zone [6]. Dashed lines correspond to nodal lines associated with $\mathbf{Q}_1$, filled circles correspond to Dirac points, empty circles to saddle points, and the thick line corresponds to the proposed CDW gap.

inside the superconducting phase [79, 79, 78], where here ϕ corresponds to the fluctuations of the secondary pairing order parameter (either is or id_{xy}). Another example is that of a proposed f-wave charge density wave (CDW) gap ($\Delta_{CDW}(\mathbf{k})$) in dichalcogenides [6], in which case the Dirac quasiparticles couple to a scalar field, ϕ, here corresponding to acoustic phonons, and the HY coupling constant g_{HY} a piezoelectric coupling. In both of these cases, the dynamical gap undergoes a phase transition driven by HY interactions, and this gap corresponds to our (2.22) above, in which $\alpha_{HY} = 0,\ \beta_{HY} = 1$.

5.1.2 Effective QED$_3$ in Condensed Matter Systems

A different way CSB may occur is when a repulsive Lorentz-invariant vector-like coupling drives Dirac fermions to undergo the symmetry-breaking transition, which, conversely, can occur for any strength of coupling g, but only if the number of fermion species $N < N_c$. This happens via the current operator $\sum_\sigma \bar{\Psi}_\sigma \hat{\gamma}_\sigma \Psi_\sigma$. Such a transition is believed to occur at the strong-coupling IR fixed point in $(2+1)$-D QED$_3$, at which $N_c \leq 3/2$ at zero temperature [54].

This CSB mechanism has been invoked to explore several formally similar, but otherwise physically different, systems. CSB in relativistic QED$_3$ theory has been adapted to describe phase transitions in underdoped cuprates, such as an antiferromagnetism to spin liquid phase and pseudogap to spin density wave [80, 81, 5, 82, 83].[2] The order parameter in each conforms directly to the framework of (2.22), corresponding to the scenario $\alpha_{QED} = \beta_{QED} = 1$.

[2]The *pseudogap* regime [84] refers to the phase in which the system first displays superconducting precursors in an underdoped regime, whereas the actual superconducting transition occurs at smaller temperatures [85].

5.2 Pairing Instability in d-wave Superconductors

In both high-T_c cuprates and heavy fermion materials – both 2D fermionic systems – as one approaches the antiferromagnetic instability, the softening of spin fluctuations causes the d-wave pairing amplitude to increase (c.f., [86, 87]), while at the same time, strong spin-mediated interactions destroy fermionic coherence [88, 89, 90], preventing Cooper pairing from taking place. Competition between these two factors yields a pairing instability at a critical temperature, which may signal the onset of a pseudogap regime [85]. This pairing problem is distinctly different from BCS pairing.

In approaching this situation, Chubukov *et al.* solved three coupled Eliashberg (integral) equations for the fermionic self-energy Σ_n, the anomalous vertex $\Phi_k(\omega)$, and the susceptibility $\chi_{\mathbf{q}}$ [85, 91, 92]. The energy-dependent (but not p-dependent) gap equation is solved in terms of these three to reveal

$$\Delta(\omega) \propto \frac{E_F}{\sqrt{\omega}} \cos\left[\beta \ln \frac{\omega}{E_F} + \phi\right]. \tag{5.4}$$

This solution, consistent with photoemission data [93, 94], agrees remarkably well with (3.18) above, in the particular conformally-invariant case $\alpha = \beta = 1/2$. Furthermore, we were able to reach essentially the same conclusions with far greater ease, without having to resort to solving a system of integral equations.

5.3 Color Superconductivity

I mention here briefly yet another system that falls under the umbrella of this research: that of color superconductivity in QCD_4. Such a case corresponds to the integral kernel in (2.22) behaving as $U(p-q) \propto \ln|p-q|$. I leave for future research additional explorations for where this may lead.

Future directions in which these analyses may be taken include generalizing to account for the transition between bulk and effectively 2D system, which is of great value to both theory

and application. Also, in chapter three we concerned ourselves entirely with singlet pairing between particles. It would be very interesting to extend the bifurcation approximation to account for *triplet* pairing.

In conclusion, the results here should be of use to a wide range of areas in condensed matter and field theory physics, particularly those involving nodal fermions. I hope that the observations here and results still developing may help elucidate many unsolved mysteries in such strongly coupled many-body phenomena.

Appendix A

Algebraic details

The following summarizes several sections from Miransky [41].

In our system, the four-component fermions live on a plane, carrying the flavor index $i = 1, 2, ..., N_f$. The Lagrangian density for the quasiparticles is

$$\mathcal{L} = v_F \bar{\Psi}\left(t, \vec{r}\right)\left[\frac{i\gamma^0\left(\partial_t + i\mu\right)}{v_F} - i\gamma^1\partial_x - i\gamma^2\partial_y\right]\Psi\left(t, \vec{r}\right) \tag{A.1}$$

where $\Psi\left(t, \vec{r}\right)$ is a four-component spinor, and $\bar{\Psi}\left(t, \vec{r}\right) = \Psi^\dagger\left(t, \vec{r}\right)\gamma^0$. The three 4×4 γ matrices can be defined as

$$\gamma^0 = \begin{pmatrix} \sigma_3 & 0 \\ 0 & -\sigma_3 \end{pmatrix}, \quad \gamma^1 = \begin{pmatrix} i\sigma_1 & 0 \\ 0 & -i\sigma_1 \end{pmatrix}, \quad \gamma^2 = \begin{pmatrix} i\sigma_2 & 0 \\ 0 & -i\sigma_2 \end{pmatrix}. \tag{A.2}$$

In $2+1$-dimensions, the two sets of matrices $(\sigma_3, i\sigma_1, i\sigma_2)$ and $(-\sigma_3, -i\sigma_1, -i\sigma_2)$ make inequivalent representations of the Clifford (Dirac) algebra,

$$\gamma^\mu\gamma^\nu + \gamma^\nu\gamma^\mu = 2g^{\mu\nu} \tag{A.3}$$

where $\mu, \nu = 0, 1, 2$ and $g^{\mu,\nu}$ =diag$(1, -1, -1)$.

There are two matrices that anticommute with γ^0, γ^1, and γ^2:

$$\gamma^3 = i\begin{pmatrix} 0 & 1 \\ 1 & 0 \end{pmatrix}, \quad \gamma^5 = i\begin{pmatrix} 0 & 1 \\ -1 & 0 \end{pmatrix}. \tag{A.4}$$

Therefore, for each four-component spinor, there is a global $U(2)$ symmetry with the generators

$$I, \quad \frac{1}{i}\gamma^3, \quad \gamma^5, \quad \frac{1}{2}\left[\gamma^3, \gamma^5\right]. \tag{A.5}$$

If we ignore relativistic corrections of order $\left(v_F/c\right)^2$, the brane action of the interacting quasiparticles is

$$\begin{aligned} S \approx \int dt d^2\vec{r}\mathcal{L}(t, \vec{r}) - \frac{1}{2}\int dt \int dt' \int d^2\vec{r} \int d^2\vec{r}' \bar{\Psi}\left(t, \vec{r}\right)\gamma^0\Psi\left(t, \vec{r}\right) \\ \times U_0\left(t - t', |\vec{r} - \vec{r}'|\right)\bar{\Psi}\left(t', \vec{r}'\right)\gamma^0\Psi\left(t', \vec{r}'\right). \end{aligned} \tag{A.6}$$

Since there are N_f fermion flavors, the full symmetry of the action (A.6) is $U(2N_f)$ with the generators

$$\frac{\lambda^\alpha}{2}, \quad \frac{\lambda^\alpha}{2i}\gamma^3, \quad \frac{\lambda^\alpha}{2}\gamma^5, \quad \frac{\lambda^\alpha}{2}\frac{1}{2}\left[\gamma^3, \gamma^5\right] \tag{A.7}$$

where $\lambda^\alpha/2$ with $\alpha = 0, 1, ..., N_f^2 - 1$ are N_f^2 generators of $U(N_f)$.

Adding a mass (gap) term $\Delta_0\bar{\psi}\psi$ into action (A.6) spontaneously breaks $U(2N_f) \to U(N_f) \times U(N_f)$, with the generators

$$\frac{\lambda^\alpha}{2}, \quad \frac{\lambda^\alpha}{2}\frac{1}{2}\left[\gamma^3, \gamma^5\right] \tag{A.8}$$

$\alpha = 0, 1, ..., N_f^2 - 1$. Hence, the dynamical generation of the fermion gap leads to this spontaneous breakdown in the symmetry of the $(2+1)$-D fermions.

Appendix B

The Bifurcation Approximation

B.1 Field Theory

We begin with the theory developed in detail in Refs[51, 95, 41]. We start with a general field theory with a spontaneously broken symmetry due to a local composite order parameter $\langle 0 \left| \bar{\psi}\psi \right| 0 \rangle \neq 0$. Here ψ is the Dirac spinor of the quasiparticle field and $\bar{\psi}$ is the (Dirac) conjugate spinor.[51]

We introduce the generating functional $W(J)$ for the Green functions of the corresponding composite field through the path integral:

$$e^{iW(J)} = \int D\psi D\bar{\psi} \exp\left\{ i \int d^3x \left[\mathcal{L}_{qp}(x) - J(x)\bar{\psi}(x)\psi(x) \right] \right\}. \tag{B.1}$$

Here $J(x)$ is the source for composite field and $\mathcal{L}_{qp}(x)$ is the Lagrangian density of quasiparticles in the model at hand.

The effective action for the field $\sigma(x) \equiv \langle 0 \left| \bar{\psi}\psi \right| 0 \rangle$ is given by the Legendre transform

$$\Gamma(\sigma) = W(J) - \int d^3x J(x)\sigma(x) \tag{B.2}$$

where $W(J)$ is the generating functional and $J(x)$ is the external source. We can express $J(x)$ in the integrand in terms of $\sigma(x)$ by inverting the relation

$$\frac{\delta W}{\delta J(x)} = \sigma(x). \tag{B.3}$$

The effective action $\Gamma(\sigma)$ describe the low-energy dynamics of the systems we are considering. Expanding this in powers of space-time derivatives of the field σ,

$$\Gamma(\sigma) = \int d^3x \left[-V(\sigma) + \frac{1}{2} Z^{\mu\nu}(\sigma)\partial_\mu\sigma\partial_\nu\sigma + ... \right] \tag{B.4}$$

where $V(\sigma)$ is the effective potential, and the "..." denote higher derivative terms and Nambu-Goldstone boson contributions. Taking eqs (B.2) and (B.3) together, we derive

$$\frac{\delta\Gamma}{\delta\sigma(x)} = -J(x). \tag{B.5}$$

As can be seen, in the limit $J(x) \to 0$, this equation becomes an equation of motion for $\sigma(x)$. Furthermore, if $J(x)$ and $\sigma(x)$ are nonzero but constant in space-time, $dV/d\sigma = 0$, and we can write the effective potential

$$V(\sigma) = -w(J) + J\sigma = \int^{\sigma} d\sigma J(\sigma) \tag{B.6}$$

where $w(J) \equiv W(J)/V_{2+1}$, V_{2+1} being the space-time volume, and here J plays the role of Δ_0, the bare gap.

The external source $J\bar{\psi}\psi$ enters the action as a quasiparticle bare mass term, and thus in the case of $J \neq 0$ (in which we have a gap) the effective potential

$$\begin{aligned} \Delta(p) - J &= \lambda \int k\ dk \frac{\Delta(k) U(p,k)}{\sqrt{k^2 + (\Delta(k)/v_F)^2}} \\ \lambda &= \frac{e^2}{2\left(\epsilon_0 v_F + \pi e^2 N_f/4\right)} \end{aligned} \tag{B.7}$$

where $U(p,k)$ is the quasiparticle interaction.

B.2 Integral equations → Differential Equations

Expanding on the technique presented above and in [41], we generalize to an arbitrary DOS and effective Coulomb interaction.

We start with the gap equation (see eqs.(2.22) and (3.1)):

$$\Delta(p) \propto \int_0^{\Lambda} k^{\beta} dk \frac{\Delta(k)}{\sqrt{k^2 + \Delta^2(k)}} \left(\frac{1}{p^{\alpha}}\right) \tag{B.8}$$

We first note that at large momenta, $\Delta \ll p \sim \Lambda$, the kernel (interaction) $U(\vec{p} - \vec{k})$ in the above integral equation can be replaced by either $U(\vec{p})$ or $U(\vec{k})$, depending on the relative magnitude of $\vec{p}$ and $\vec{k}$. Then, we make a change of variable from the momentum $\vec{p}$ to energy $\epsilon = E_p$ (via the energy dispersion) and split the integral into two portions:

$$\Delta_p = \underbrace{\lambda h_0 \int_0^{p} k^{\beta} dk \frac{\Delta_k}{\sqrt{k^2 + \Delta_k^2}} \left(\frac{1}{p^{\alpha}}\right)}_{\Delta_<(p)} + \underbrace{\lambda h_0 \int_p^{\Lambda} k^{\beta} dk \frac{\Delta_k}{\sqrt{k^2 + \Delta_k^2}} \left(\frac{1}{k^{\alpha}}\right)}_{\Delta_>(p)}. \tag{B.9}$$

Hence,

$$\Delta\left(p\right) = \Delta_<\left(p\right) + \Delta_>\left(p\right) \tag{B.10}$$

and thus,

$$\Delta'_<\left(p\right) = -\lambda h_0 p^{\beta-\alpha} \frac{\Delta_p}{\sqrt{p^2 + \Delta_p^2}}$$

In the large momentum limit $p \gg \Delta$ we may ignore Δ in the denominator, making this

$$= -\lambda h_0 \frac{\Delta_p}{p^{1+\alpha-\beta}}. \tag{B.11}$$

Likewise,

$$\begin{aligned}
\Delta'_< (p) &= \lambda h_0 \left(\frac{-\alpha}{p^{\alpha+1}}\right) \int_0^p dk \frac{k^\beta \Delta_k}{\sqrt{k^2+\Delta_k^2}} + \lambda h_0 \frac{p^\beta \Delta_p}{\sqrt{p^2+\Delta_p^2}} \frac{1}{p^\alpha} \\
&\to \lambda h_0 \frac{-\alpha}{p^{\alpha+1}} \int_0^p dk \frac{k^\beta \Delta_k}{\sqrt{k^2+\Delta_k^2}} + \lambda h_0 \frac{\Delta_p}{p^{1+\alpha-\beta}} \\
&\Rightarrow \Delta'_< = \frac{-\alpha}{p} \Delta_< (p) + \lambda h_0 \frac{\Delta_p}{p^{1+\alpha-\beta}}
\end{aligned} \tag{B.12}$$

so

$$\Delta' = \Delta'_< + \Delta'_> = \left(\frac{-\alpha}{p}\right) \Delta_< (p) . \tag{B.13}$$

Thus,

$$\begin{aligned}
\Delta'' &= \frac{+\alpha}{p^2} \Delta_< (p) - \frac{\alpha}{p} \Delta'_< (p) \\
&= \frac{\alpha}{p^2} \Delta_< (p) - \frac{\alpha}{p} \left(\frac{-\alpha}{p}\right) \Delta_< (p) - \lambda h_0 \alpha \frac{\Delta_p}{p^{1+\alpha-\beta}} \\
&= \frac{\alpha (\alpha+1)}{p^2} \Delta_< - \lambda h_0 \alpha \frac{\Delta}{p^{2+\alpha-\beta}}.
\end{aligned} \tag{B.14}$$

Substituting in our above result for Δ', we get

$$= \frac{\alpha (\alpha+1)}{p^2} \left(\frac{-p}{\alpha}\right) \Delta' - \frac{\lambda h_0 \alpha}{p^{2+\alpha-\beta}} \Delta.$$

Hence,

$$\Delta'' + \frac{\alpha+1}{p} \Delta' + \frac{\lambda h_0 \alpha}{p^{2+\alpha-\beta}} \Delta = 0 \tag{B.15}$$

which is eq.(3.6) above.

B.3 Free Energy

In light of the above differential equation, we also take into account the infrared boundary condition

$$p^2 \Delta'(p)\big|_{p=\Delta/v_F} = 0, \tag{B.16}$$

the ultraviolet boundary condition

$$J = \left(\Delta(p) + p\Delta'(p)\right)\big|_{p=\Lambda}, \tag{B.17}$$

and the relation for the composite field

$$\sigma(\Delta) = -\left\langle \bar{\psi}\psi \right\rangle = -\frac{N_f}{\pi\lambda v_F} p^2 \Delta'(p)\Big|_{p=\Lambda}. \tag{B.18}$$

From these and (B.6), we rewrite the effective potential dependent on Δ, and thus determine the free energy

$$F(\Delta) = V\left(\sigma(\Delta)\right) = \int^{\Delta} d\Delta' \frac{d\sigma(\Delta)}{d\Delta} J(\Delta). \tag{B.19}$$

We will use these methods extensively in subsequent analysis to determine the nature of quantum phase transitions in nodal fermion systems.

Appendix C

Quantum Phase Transitions of the Free Energy

C.1 Example: $\alpha = \beta = 1$

As a detailed example of a conformally (scale) invariant non-BCS system, consider the scenario $\alpha = \beta = 1$ (i.e., having a DOS $\nu(\epsilon) \propto \epsilon$, and long-ranged (bare) interaction potential $U^{(0)}(\mathbf{q}) = g_0/q$).

C.1.1 $\eta = 1$

We begin with the case of a linear dispersion $\xi_p \propto p$. The solution to the gap equation (3.6) is given by

$$\Delta_p = \begin{cases} \frac{\Delta}{\sin\delta}\sqrt{\frac{\Delta}{p}}\sin\left[\sqrt{g-1/4}\ln\frac{p}{\Delta}+\delta\right], & \mu \le \Delta \\ \frac{\Delta}{\sin\left[\sqrt{g-1/4}\ln\frac{\mu}{\Delta}+\delta\right]}\sqrt{\frac{\mu}{p}}\sin\left[\sqrt{g-1/4}\ln\frac{p}{\Delta}+\delta\right], & \mu > \Delta \end{cases} \tag{C.1}$$

where the phase δ is to be fixed by the IR boundary condition. Focusing on the $\mu \le \Delta$, the IR boundary condition

$$\begin{aligned} \left.\frac{d\Delta(\epsilon)}{d\epsilon}\right|_{\epsilon=\Delta} &= 0 \\ \Rightarrow \delta &= \sqrt{4g-1}. \end{aligned} \tag{C.2}$$

The UV boundary condition fixes the UV cutoff, $\Lambda \sim$ span of the Brillouin zone, in terms of Δ,

$$\begin{aligned} \Delta(\epsilon) + \epsilon\left.\frac{d\Delta(\epsilon)}{d\epsilon}\right|_{\epsilon=\Lambda} &= 0 \\ \Rightarrow \Lambda = \Delta_0 \exp\frac{\pi - 2\delta}{\sqrt{g-1/4}}. \end{aligned} \tag{C.3}$$

Thus, the current

$$J(\Delta) = \Delta(\epsilon) + \epsilon \frac{d\Delta(\epsilon)}{d\epsilon}\bigg|_{p=\Lambda}$$
$$= -\frac{\Delta}{2\sqrt{4g-1}}\sqrt{\frac{\Delta}{\Lambda}}\left[\sqrt{4g-1}\cos\left(\frac{\sqrt{4g-1}}{2}\ln\frac{\Delta_0}{\Delta} - \sqrt{4g-1}\right)\right.$$
$$\left. + \sin\left(\frac{\sqrt{4g-1}}{2}\ln\frac{\Delta_0}{\Delta} - \sqrt{4g-1}\right)\right], \tag{C.4}$$

which, as $g \to g_c = 1/4$ and writing Λ in terms of Δ_0 in the oscillating term,

$$J(\Delta) \approx -\frac{\Delta}{4}\sqrt{\frac{\Delta}{\Lambda}}\ln\frac{\Delta_0}{\Delta}. \tag{C.5}$$

Likewise, for $\mu > \Delta$, given that the relations for the IR and UV boundary conditions are the same as for $\mu < \Delta$,

$$J(\Delta,\mu) = \frac{-\Delta}{2\sin\left[\frac{\sqrt{4g-1}}{2}\ln\frac{\mu}{\Delta} + \sqrt{4g-1}\right]}\sqrt{\frac{\mu}{\Lambda}}\left[\sqrt{4g-1}\cos\left(\frac{\sqrt{4g-1}}{2}\ln\frac{\Delta_0}{\Delta} - \sqrt{4g-1}\right)\right.$$
$$\left. + \sin\left(\frac{\sqrt{4g-1}}{2}\ln\frac{\Delta_0}{\Delta} - \sqrt{4g-1}\right)\right]$$

which, again as $g \to g_c$

$$J(\Delta) \approx -\frac{\Delta}{2\ln\frac{\mu}{\Delta} + 4}\sqrt{\frac{\mu}{\Lambda}}\ln\frac{\Delta_0}{\Delta} \quad . \tag{C.6}$$

The order parameter for $\mu < \Delta$

$$\sigma(\Delta) = -\frac{\epsilon^{\alpha+1}}{\alpha g_0}\frac{d\Delta(\epsilon)}{d\epsilon}\bigg|_{\epsilon=\Lambda}$$
$$= \frac{\Delta\sqrt{\Delta\Lambda}}{2\sin\sqrt{4g-1}}\left[\sin\left(\frac{\sqrt{4g-1}}{2}\ln\frac{\Lambda}{\Delta} + \sqrt{4g-1}\right)\right.$$
$$\left. - \sqrt{4g-1}\cos\left(\frac{\sqrt{4g-1}}{2}\ln\frac{\Lambda}{\Delta} + \sqrt{4g-1}\right)\right], \tag{C.7}$$

and

$$\frac{d\sigma}{d\Delta} = \frac{\sqrt{\Delta\Lambda}}{\sin\sqrt{4g-1}}\left[\sqrt{4g-1}\cos\left(\frac{\sqrt{4g-1}}{2}\ln\frac{\Delta_0}{\Delta} - \sqrt{4g-1}\right)\right.$$
$$\left. + (g-1)\sin\left(\frac{\sqrt{4g-1}}{2}\ln\frac{\Delta_0}{\Delta} - \sqrt{4g-1}\right)\right] \tag{C.8}$$
$$\overset{g\to g_c}{\approx} \sqrt{\Delta\Lambda}\left(\frac{7}{4} - \frac{3}{8}\ln\frac{\Delta_0}{\Delta}\right) \tag{C.9}$$

whereas for $\mu > \Delta$,

$$\frac{d\sigma(\Delta,\mu)}{d\Delta} \approx \frac{\sqrt{\mu\Lambda}}{2\ln\frac{\mu}{\Delta} + 4}\left(\ln\frac{\Delta_0}{\Delta} - 5\right). \tag{C.10}$$

Thus, the free energy

$$\begin{aligned} F(\Delta,\mu) &= \int_0^\Delta d\Delta' \frac{d\sigma}{d\Delta'} J(\Delta') + F(0,\mu) \\ &= \int_0^\mu d\Delta' \frac{d\sigma(\Delta',\mu)}{d\Delta'} J(\Delta',\mu) + \int_\mu^\Delta d\Delta' \frac{d\sigma(\Delta')}{d\Delta'} J(\Delta') + F(0,\mu) \\ &= \int_0^\mu d\Delta' \frac{\Delta'\mu}{4\left(\ln\frac{\mu}{\Delta'}+2\right)^2} \ln\frac{\Delta_0}{\Delta'}\left(\ln\frac{\Delta_0}{\Delta'}-5\right) \\ &\qquad - \int_\mu^\Delta d\Delta' \frac{(\Delta')^2}{4} \ln\frac{\Delta_0}{\Delta'}\left(\frac{7}{4}-\frac{3}{8}\ln\frac{\Delta_0}{\Delta'}\right) + F(0,\mu). \end{aligned} \tag{C.11}$$

(C.12)

Noting that the integration constant

$$\frac{\partial F(\Delta,\mu)}{\partial\mu} = -n(\mu) = \sum_{\vec{p},\mp} \theta(\mu \mp E_p),$$

where $n(\mu)$ is the density of excess particles, the free energy functional

$$F(\Delta,\mu) = \frac{g}{2g_0}\left[I_<(\Delta,\mu) - I_<(\Delta_0,\mu) - \frac{1}{2}\int_\Delta^\mu d\omega(\omega^2-\Delta^2)\right] \tag{C.13}$$

where

$$I_<(\Delta,\mu) = \mu\int_0^\mu d\omega\omega \frac{\ln(\Delta_0/\omega)[5-\ln(\Delta_0/\omega)]}{(2+\ln\mu/\omega)^2}, \tag{C.14}$$

whereas for $\Delta > \mu$ we have

$$F_>(\Delta,\mu) = \frac{g}{2g_0}\left[I_>(\Delta,\mu) - I_>(\mu,\mu) + I_<(\mu,\mu) - I_<(\Delta_0,\mu)\right] \tag{C.15}$$

where

$$I_>(\Delta,\mu) = -\frac{2}{3}\Delta^3 - 2\Delta^3\ln\frac{\Delta_0}{\Delta} + \frac{\Delta^3}{2}\ln^2\frac{\Delta_0}{\Delta} \tag{C.16}$$

which is the result cited in chapter 2.

Explicitly,

$$\begin{aligned} \frac{g}{2g_0}I_< = \frac{\mu}{8}\Big\{ &\Delta^2 + 74e^4\mu^2 Ei\left[-2\ln\frac{\mu}{\Delta}-4\right] + 40e^4\mu^2\ln\mu\ Ei\left[-2\ln\frac{\mu}{\Delta}-4\right] \\ &+4e^4\mu^2\ln^2\mu\ Ei\left[-2\ln\frac{\mu}{\Delta}-4\right] + \frac{2\Delta^2\left(14+9\ln\mu+\ln^2\mu\right)}{2+\ln\frac{\mu}{\Delta}}\Big\} \end{aligned} \tag{C.17}$$

where $Ei(z)$ is the exponential integral function

$$Ei(z) = \int_z^\infty \frac{e^{-t}}{t}dt.$$

Plotting $F(\Delta)$ vs. Δ for several values of μ, we see in fig.3.4 that $\mu_c \approx 0.6$.

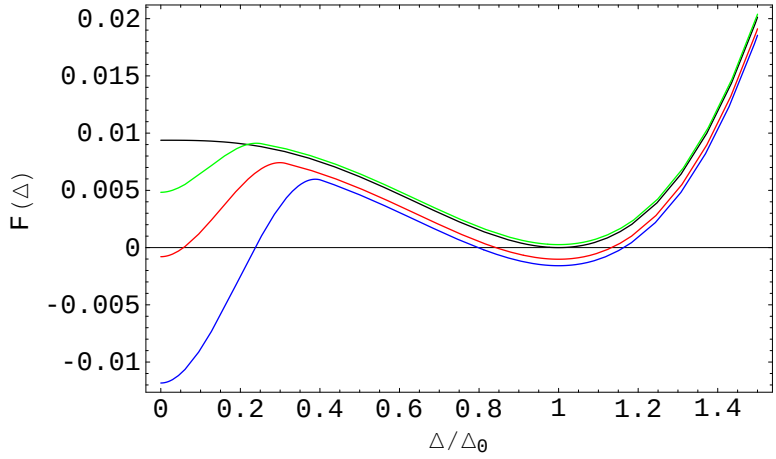

Figure C.1: Free energy for $\alpha = \beta = 1$, and $\eta = 1/2$ as a function of chemical potential μ (in units of Δ_0): 0 (black), 0.25 (green), 0.31 (red), and 0.4 (blue).

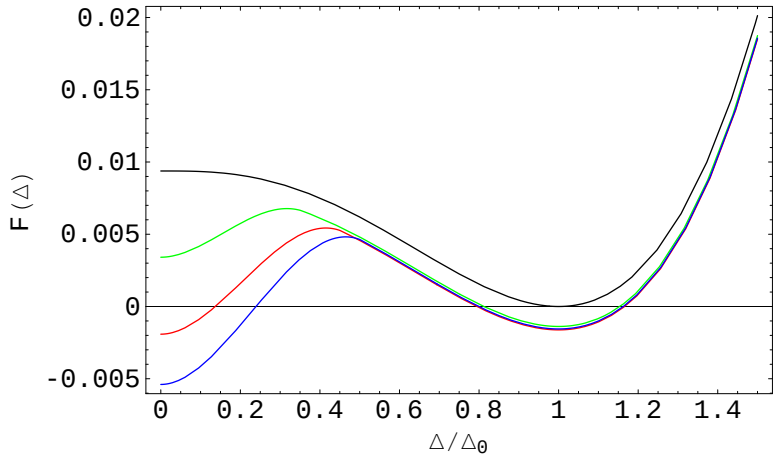

Figure C.2: Free energy for $\alpha = \beta = 1$, and $\eta = 3/2$ as a function of chemical potential μ (in units of Δ_0): 0 (black), 0.35 (green), 0.45 (red), and 0.5 (blue).

C.1.2 General η

As mentioned before, the above results correspond to the parameter η such that $\xi_p \propto p^{\eta=1}$. We can account for more general energy dispersion by allowing η to vary, holding β constant. After repeating the above analysis, we find the following free energy phase transitions:

For $\eta = 1/2$, we see from the free energy plot (fig.C.1) that the critical chemical potential $\mu_c \approx 0.31$. Likewise, for $\eta = 3/2$, $\mu_c \approx 0.45$ (fig.C.2), and for $\eta = 2$, $\mu_c \approx 0.49$ (fig.C.3). Fitting the plot of μ_c vs. η, we find that $\mu_c = -0.04\eta^2 + 0.22\eta + 0.21$ for $\alpha = \beta = 1$.

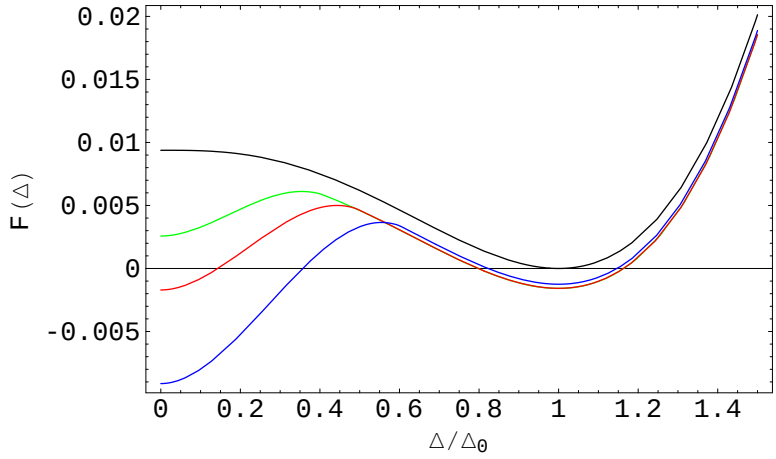

Figure C.3: Free energy for $\alpha = \beta = 1$, and $\eta = 2$ as a function of chemical potential μ (in units of Δ_0): 0 (black), 0.4 (green), 0.49 (red), and 0.6 (blue).

C.2 Example: $\alpha = 1/2,\ \beta = 1$

As an example of a more general $\alpha < \beta$ system, consider the scenario $\alpha = 1/2,\ \beta = 1$, which still corresponds to a linear DOS ($\nu(\epsilon) \propto \epsilon$) and energy dispersion ($\xi_p \propto p,\ \eta = 1$), but now with an interaction $U^{(0)}(\mathbf{q}) = g_0/\sqrt{q}$.

The general solution to the gap equation becomes

$$\Delta_p = \frac{\sqrt{9 + 32g\sqrt{\Delta}}}{4\sqrt{2g\sqrt{\Delta}}}\Delta\left(\frac{\Delta}{p}\right)^{3/8}\sin\left\{\frac{1}{2}\sqrt{2g\sqrt{p}-3}\left[1-(\Delta/p)^{1/4}\right] + \arctan\left[\frac{4}{3}\sqrt{2g\sqrt{\Delta}}\right]\right\} \tag{C.18}$$

for $\mu \leq \Delta$, and

$$\Delta_p = \frac{\Delta}{\sin\left[\frac{1}{2}\sqrt{2g\sqrt{\mu}-3}\left[1-(\Delta/\mu)^{1/4}\right] + \arctan\left[\frac{4}{3}\sqrt{2g\sqrt{\Delta}}\right]\right]} \times\left(\frac{\mu}{p}\right)^{3/8}\sin\left\{\frac{1}{2}\sqrt{2g\sqrt{p}-3}\left[1-(\Delta/p)^{1/4}\right] + \arctan\left[\frac{4}{3}\sqrt{2g\sqrt{\Delta}}\right]\right\} \tag{C.19}$$

for $\Delta < \mu$, where

$$\delta \approx \begin{cases} \arctan\frac{4\sqrt{2g}}{3} = \arctan\frac{4\sqrt{2\tilde{g}\sqrt{\Delta/\Lambda}}}{3}\ , & \Delta \sim 1 \gg 0 \\ 0\ , & \Delta \ll 1 \end{cases} \tag{C.20}$$

is the solution to the IR boundary condition, and $\tilde{g}$ is the dimensionless coupling constant.

A subtlety is that now we are dealing with a *non*-conformally invariant system. Conformal invariance implies that the coupling g is dimensionless, and thus $J(\Delta)$ and $\sigma(\Delta)$ are independent of g. On the other hand, in the case of $\alpha < \beta$, g is now p-dependent, or rather, in the bifurcation approximation ($p \to \Lambda$), is in units of $\Lambda^{\alpha-\beta}$. Hence, g cannot be eliminated from $J(\Delta)$ or $\sigma(\Delta)$. Thus, we must rewrite the coupling as a dimensionless quantity, $\tilde{g} = g\Lambda^{\beta-\alpha}$.

The UV boundary condition yields

$$\Delta_0 \approx 17\Lambda \left(g - g_c\right)^4 \tag{C.21}$$

and the current for $\mu < \Delta$

$$\begin{aligned} J(\Delta) = {} & \frac{\sqrt{18 + 64g\sqrt{\Delta}}}{32\sqrt{g\sqrt{\Delta}}} \Delta \left(\frac{\Delta}{\Lambda}\right)^{3/8} \\ & \times \left\{ \left[\frac{32g\sqrt{\Lambda} - 3\left(\Delta/\Lambda\right)^{1/4}}{\sqrt{32g\sqrt{\Lambda} - 3}} \right] \cos \left[\frac{\sqrt{32g\sqrt{\Lambda} - 3}}{2} \left(1 - \left(\frac{\Delta}{\Lambda}\right)^{1/4}\right) + \arctan\left(\frac{\sqrt{32g\sqrt{\Delta}}}{3}\right) \right] \right. \\ & \left. + \sin \left[\frac{\sqrt{32g\sqrt{\Lambda} - 3}}{2} \left(1 - \left(\frac{\Delta}{\Lambda}\right)^{1/4}\right) + \arctan\left(\frac{\sqrt{32g\sqrt{\Delta}}}{3}\right) \right] \right\} \end{aligned}$$

where the simplification

$$\csc\left[\arctan\frac{\sqrt{32g\sqrt{\Delta}}}{3}\right] = \frac{\sqrt{9 + 32g\sqrt{\Delta}}}{\sqrt{32g\sqrt{\Delta}}} \tag{C.22}$$

specifically in the case of $\alpha = 1/2,\ \mu = 0$.
For $\Delta < \mu$

$$\begin{aligned} J(\Delta) = {} & \frac{\Delta}{4}\left(\frac{\mu}{\Lambda}\right)^{3/8} \csc\left[\frac{\sqrt{32g\sqrt{\mu} - 3}}{2} \left(1 - \left(\frac{\Delta}{\mu}\right)^{1/4}\right) + \arctan\left(\frac{\sqrt{32g\sqrt{\Delta}}}{3}\right) \right] \\ & \times \left\{ \left[\frac{32g\sqrt{\Lambda} - 3\left(\Delta/\Lambda\right)^{1/4}}{\sqrt{32g\sqrt{\Lambda} - 3}} \right] \cos \left[\frac{\sqrt{32g\sqrt{\Lambda} - 3}}{2} \left(1 - \left(\frac{\Delta}{\Lambda}\right)^{1/4}\right) + \arctan\left(\frac{\sqrt{32g\sqrt{\Delta}}}{3}\right) \right] \right. \\ & \left. + \sin \left[\frac{\sqrt{32g\sqrt{\Lambda} - 3}}{2} \left(1 - \left(\frac{\Delta}{\Lambda}\right)^{1/4}\right) + \arctan\left(\frac{\sqrt{32g\sqrt{\Delta}}}{3}\right) \right] \right\} \end{aligned}$$

Note that we are not able to simplify these further (i.e., the oscillating terms) as we had in the conformally invariant case.

Similarly the order parameter for $\mu < \Delta$

$$\sigma(\Delta) = -\frac{\sqrt{18+64g\sqrt{\Delta}}}{32\sqrt{g\sqrt{\Delta}}}\Delta\sqrt{\Lambda}\left(\frac{\Delta}{\Lambda}\right)^{3/8} \times\left\{\left[\frac{32g\sqrt{\Lambda}-3\left(\Delta/\Lambda\right)^{1/4}}{\sqrt{32g\sqrt{\Lambda}-3}}\right]\cos\left[\frac{\sqrt{32g\sqrt{\Lambda}-3}}{2}\left(1-\left(\frac{\Delta}{\Lambda}\right)^{1/4}\right)+\arctan\left(\frac{\sqrt{32g\sqrt{\Delta}}}{3}\right)\right]\right.$$
$$\left.-3\sin\left[\frac{\sqrt{32g\sqrt{\Lambda}-3}}{2}\left(1-\left(\frac{\Delta}{\Lambda}\right)^{1/4}\right)+\arctan\left(\frac{\sqrt{32g\sqrt{\Delta}}}{3}\right)\right]\right\}$$

whereas for $\Delta < \mu$

$$\sigma(\Delta) = \frac{\Delta\sqrt{\Lambda}}{4}\left(\frac{\mu}{\Lambda}\right)^{3/8}\csc\left[\frac{\sqrt{32g\sqrt{\mu}-3}}{2}\left(1-\left(\frac{\Delta}{\mu}\right)^{1/4}\right)+\arctan\left(\frac{\sqrt{32g\sqrt{\Delta}}}{3}\right)\right] \times\left\{3\sin\left[\frac{\sqrt{32g\sqrt{\Lambda}-3}}{2}\left(1-\left(\frac{\Delta}{\Lambda}\right)^{1/4}\right)+\arctan\left(\frac{\sqrt{32g\sqrt{\Delta}}}{3}\right)\right]\right.$$
$$\left.-\left[\frac{32g\sqrt{\Lambda}-3\left(\Delta/\Lambda\right)^{1/4}}{\sqrt{32g\sqrt{\Lambda}-3}}\right]\cos\left[\frac{\sqrt{32g\sqrt{\Lambda}-3}}{2}\left(1-\left(\frac{\Delta}{\Lambda}\right)^{1/4}\right)+\arctan\left(\frac{\sqrt{32g\sqrt{\Delta}}}{3}\right)\right]\right\}.$$

The UV boundary condition imposes that $\Delta_0 \approx 17\Lambda(\tilde{g}-\tilde{g}_c)^4$ where $\tilde{g}_c \approx 0.495687$.
We focus on each value of the chemical potential, μ, at a time. Expanding around the maximum gap $\Delta = 1$ in the slowly varying decaying (oscillating) terms in the current $J(\Delta)$ and derivative of the order parameter, $d\sigma/d\Delta$ – but, importantly, keeping the prefactor in its original form – we find the free energy for $\mu \leq \Delta$

$$F(\Delta) \approx \sqrt{6.4\sqrt{\Delta}}\Big[1.776\times10^{-15}+1.421\times10^{-14}\sqrt{\Delta}-1.776\times10^{-14}\Delta +1.066\times10^{-14}\Delta^{3/2}-0.07466\times\Delta^2 +4.441\times10^{-16}\Delta^{5/2}+0.07421\Delta^3-0.02070\Delta^4 +6.939\times10^{-18}\Delta^{-9/2}+0.002844\Delta^5\Big] \tag{C.23}$$

and, as an example for $\mu > \Delta$, here $\mu = 1/2$, we find

$$F(\Delta,\mu=1/2) \approx 0.002670\Big[602.5\sqrt{\Delta}-214.2\Delta+101.6\Delta^{3/2}-137.5\Delta^2 +78.21\Delta^{5/2}+34.18\Delta^3-20.83\Delta^{7/2}-19.17\Delta^4 +12.11\Delta^{9/2}+7.916\Delta^5-5.117\Delta^{11/2}-1.523\Delta^6 +\Delta^{13/2}-847.2\ln\left(\sqrt{\Delta}+1.406\right)\Big] \tag{C.24}$$

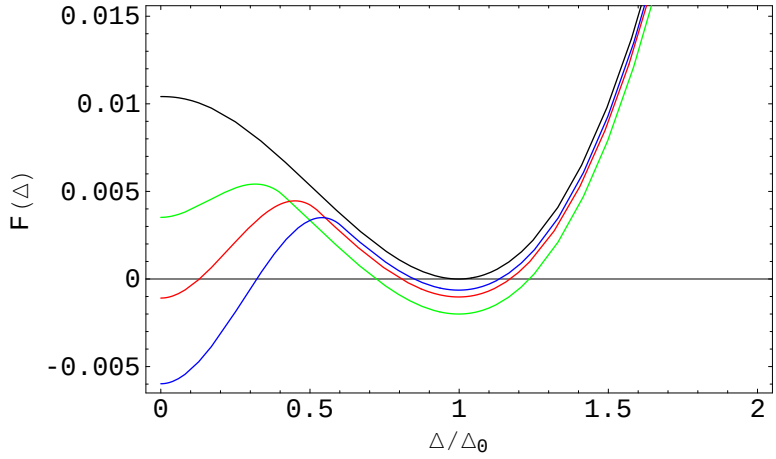

Figure C.4: Free energy for $\alpha = 1/2$, $\beta = 1$, and $\eta = 2$ as a function of chemical potential μ (in units of Δ_0): 0 (black), 0.4 (green), 0.52 (red), and 0.6 (blue).

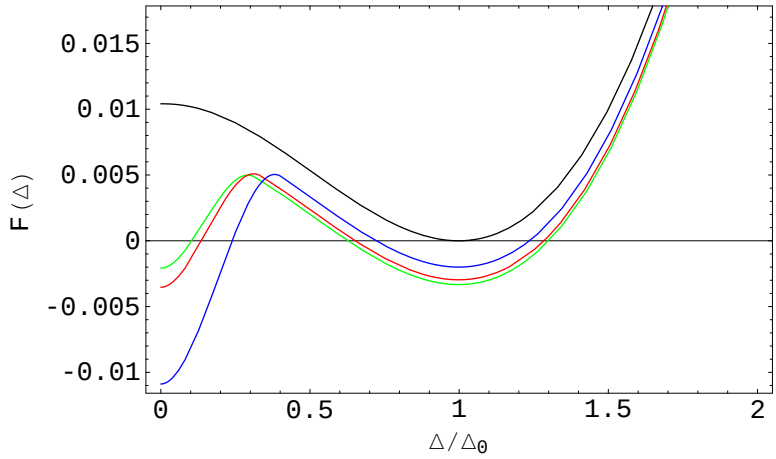

Figure C.5: Free energy for $\alpha = 1/2$, $\beta = 1$, and $\eta = 1/2$ as a function of chemical potential μ (in units of Δ_0): 0 (black), 0.3 (green), 0.33 (red), and 0.4 (blue).

We see from the plots for the free energy, $F(\Delta, \mu)$, for various values of μ (fig.3.5) that $\mu_c \approx 0.665$.

C.2.1 General η

As in the $\alpha = \beta = 1$ case, we can generalize to a more general energy dispersion here as well. For $\eta = 2$, we see from the free energy plot (fig.C.4) that the critical chemical potential $\mu_c \approx 0.52$. Likewise, for $\eta = 1/2$, $\mu_c \approx 0.33$ (fig.C.5), and for $\eta = 3/2$, $\mu_c \approx 0.47$ (fig.C.6).

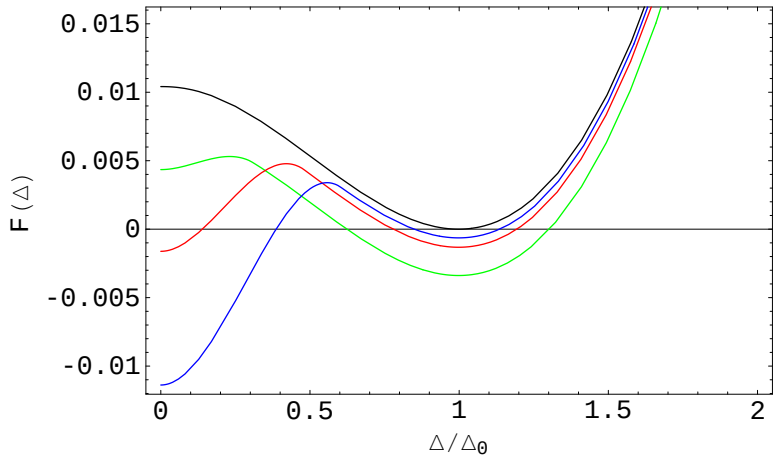

Figure C.6: Free energy for $\alpha = 1/2$, $\beta = 1$, and $\eta = 3/2$ as a function of chemical potential μ (in units of Δ_0): 0 (black), 0.3 (green), 0.475 (red), and 0.6 (blue).

Fitting the plot of μ_c vs. η, we find that $\mu_c = -0.03\eta^2 + 0.201\eta + 0.2375$ for $\alpha = 1/2,\ \beta = 1$.

C.3 Example: $\alpha = 2/3,\ \beta = 1$

For another $\beta/3 < \alpha < \beta$ case, we find similar phenomena here as in the $\alpha = 1/2,\ \beta = 1$ scenario. In the case of $\alpha = 2/3,\ \beta = 1$, the gap for $\Delta \geq \mu$ is

$$\Delta_p = \Delta\sqrt{\frac{4}{24g\Delta^{1/3} - 3} + 1}\left(\frac{\Delta}{p}\right)^{5/12} \times \sin\left\{\sqrt{\frac{2gp^{1/3}}{3} - \frac{5}{48}}\frac{\left[1 - (\Delta/p)^{1/6}\right]}{1/6} + \arctan\left[\frac{\sqrt{24g\Delta^{1/3} - 3}}{2}\right]\right\} \quad \text{(C.25)}$$

whereas for $\Delta < \mu$

$$\Delta_p = \Delta\left(\frac{\mu}{p}\right)^{5/12} \frac{\sin\left\{\sqrt{\frac{2gp^{1/3}}{3} - \frac{5}{48}}\frac{\left[1-(\Delta/p)^{1/6}\right]}{1/6} + \arctan\left[\frac{\sqrt{24g\Delta^{1/3}-3}}{2}\right]\right\}}{\sin\left\{\sqrt{\frac{2g\mu^{1/3}}{3} - \frac{5}{48}}\frac{\left[1-(\Delta/\mu)^{1/6}\right]}{1/6} + \arctan\left[\frac{\sqrt{24g\Delta^{1/3}-3}}{2}\right]\right\}} \quad \text{(C.26)}$$

where the phase

$$\delta = \begin{cases} \arctan\left[\frac{\sqrt{24g\Delta^{1/3}-3}}{2}\right], & \Delta \geq \left(\frac{1}{8g}\right)^3 \text{ or } g \geq \frac{1}{8\Delta^{1/3}} \\ 0, & \Delta < \left(\frac{1}{8g}\right)^3 \text{ or } g < \frac{1}{8\Delta^{1/3}} \end{cases} \quad \text{(C.27)}$$

satisfies the IR boundary condition. Likewise, the UV boundary condition imposes that $\Delta_0 \approx 44\Lambda(\tilde{g} - \tilde{g}_c)^6$ where $\tilde{g}_c \approx 0.3131$. For $\mu \leq \Delta$, the current

$$J(\Delta) = \frac{\Delta}{8}\left(\frac{\Delta}{\Lambda}\right)^{5/12}\sqrt{\frac{24g\Delta^{1/3}+1}{8g\Delta^{1/3}-1}}$$
$$\times\left\{\left[\frac{32g\Lambda^{1/3}-5\left(\Delta/\Lambda\right)^{1/6}}{\sqrt{32g\Lambda^{1/3}-5}}\right]\cos\left[\sqrt{\frac{2}{3}g\Lambda^{1/3}-\frac{5}{48}}\left(\frac{1-(\Delta/\Lambda)^{1/6}}{1/6}\right)+\arctan\left(\frac{\sqrt{24g\Delta^{1/3}-3}}{2}\right)\right]\right.$$
$$\left.+\sqrt{3}\sin\left[\sqrt{\frac{2}{3}g\Lambda^{1/3}-\frac{5}{48}}\left(\frac{1-(\Delta/\Lambda)^{1/6}}{1/6}\right)+\arctan\left(\frac{\sqrt{24g\Delta^{1/3}-3}}{2}\right)\right]\right\}$$

whereas for $0.0637 < \Delta < \mu$,

$$J(\Delta) = \frac{\sqrt{3}}{8}\Delta\left(\frac{\mu}{\Lambda}\right)^{5/12}\csc\left[\sqrt{\frac{2}{3}g\mu^{1/3}-\frac{5}{48}}\left(\frac{1-(\Delta/\mu)^{1/6}}{1/6}\right)+\arctan\left(\frac{\sqrt{24g\Delta^{1/3}-3}}{2}\right)\right]$$
$$\times\left\{\left[\frac{32g\Lambda^{1/3}-5\left(\Delta/\Lambda\right)^{1/6}}{\sqrt{32g\Lambda^{1/3}-5}}\right]\cos\left[\sqrt{\frac{2}{3}g\Lambda^{1/3}-\frac{5}{48}}\left(\frac{1-(\Delta/\Lambda)^{1/6}}{1/6}\right)+\arctan\left(\frac{\sqrt{24g\Delta^{1/3}-3}}{2}\right)\right]\right.$$
$$\left.+\sqrt{3}\sin\left[\sqrt{\frac{2}{3}g\Lambda^{1/3}-\frac{5}{48}}\left(\frac{1-(\Delta/\Lambda)^{1/6}}{1/6}\right)+\arctan\left(\frac{\sqrt{24g\Delta^{1/3}-3}}{2}\right)\right]\right\}$$

and for $\Delta < 0.0637 < \mu$ (where $\delta = 0$),

$$J(\Delta) = \frac{\sqrt{3}}{8}\Delta\left(\frac{\mu}{\Lambda}\right)^{5/12}\csc\left[\sqrt{\frac{2}{3}g\mu^{1/3}-\frac{5}{48}}\left(\frac{1-(\Delta/\mu)^{1/6}}{1/6}\right)\right]$$
$$\times\left\{\left[\frac{32g\Lambda^{1/3}-5\left(\Delta/\Lambda\right)^{1/6}}{\sqrt{32g\Lambda^{1/3}-5}}\right]\cos\left[\sqrt{\frac{2}{3}g\Lambda^{1/3}-\frac{5}{48}}\left(\frac{1-(\Delta/\Lambda)^{1/6}}{1/6}\right)\right]\right.$$
$$\left.+\sqrt{3}\sin\left[\sqrt{\frac{2}{3}g\Lambda^{1/3}-\frac{5}{48}}\left(\frac{1-(\Delta/\Lambda)^{1/6}}{1/6}\right)\right]\right\}.$$

Likewise, the order parameter for $\mu \leq \Delta$

$$\sigma(\Delta) = \Delta^{17/12}\Lambda^{1/4}\frac{\sqrt{3}}{24}\sqrt{\frac{24g\Delta^{1/3}+1}{8g\Delta^{1/3}-1}}$$
$$\times\left\{-\sqrt{3}\left[\frac{32g\Lambda^{1/3}-5(\Delta/\Lambda)^{1/6}}{\sqrt{32g\Lambda^{1/3}-5}}\right]\cos\left[\sqrt{\frac{2}{3}g\Lambda^{1/3}-\frac{5}{48}}\left(\frac{1-(\Delta/\Lambda)^{1/6}}{1/6}\right)+\arctan\left(\frac{\sqrt{24g\Delta^{1/3}-3}}{2}\right)\right]\right.$$
$$\left.+5\sin\left[\sqrt{\frac{2}{3}g\Lambda^{1/3}-\frac{5}{48}}\left(\frac{1-(\Delta/\Lambda)^{1/6}}{1/6}\right)+\arctan\left(\frac{\sqrt{24g\Delta^{1/3}-3}}{2}\right)\right]\right\},$$

for $\Delta < \mu$

$$\sigma(\Delta) = \frac{1}{8}\Delta\Lambda^{2/3}\left(\frac{\mu}{\Lambda}\right)^{5/12}\csc\left[\sqrt{\frac{2}{3}g\mu^{1/3}-\frac{5}{48}}\left(\frac{1-(\Delta/\mu)^{1/6}}{1/6}\right)+\arctan\left(\frac{\sqrt{24g\Delta^{1/3}-3}}{2}\right)\right]$$
$$\times\left\{\sqrt{3}\left[\frac{32g\Lambda^{1/3}-5(\Delta/\Lambda)^{1/6}}{\sqrt{32g\Lambda^{1/3}-5}}\right]\cos\left[\sqrt{\frac{2}{3}g\Lambda^{1/3}-\frac{5}{48}}\left(\frac{1-(\Delta/\Lambda)^{1/6}}{1/6}\right)+\arctan\left(\frac{\sqrt{24g\Delta^{1/3}-3}}{2}\right)\right]\right.$$
$$\left.+5\sin\left[\sqrt{\frac{2}{3}g\Lambda^{1/3}-\frac{5}{48}}\left(\frac{1-(\Delta/\Lambda)^{1/6}}{1/6}\right)+\arctan\left(\frac{\sqrt{24g\Delta^{1/3}-3}}{2}\right)\right]\right\},$$

and for $\Delta < 0.0637 < \mu$

$$\sigma(\Delta) = \frac{1}{8}\Delta\Lambda^{2/3}\left(\frac{\mu}{\Lambda}\right)^{5/12}\csc\left[\sqrt{\frac{2}{3}g\mu^{1/3}-\frac{5}{48}}\left(\frac{1-(\Delta/\mu)^{1/6}}{1/6}\right)\right]$$
$$\times\left\{\sqrt{3}\left[\frac{32g\Lambda^{1/3}-5(\Delta/\Lambda)^{1/6}}{\sqrt{32g\Lambda^{1/3}-5}}\right]\cos\left[\sqrt{\frac{2}{3}g\Lambda^{1/3}-\frac{5}{48}}\left(\frac{1-(\Delta/\Lambda)^{1/6}}{1/6}\right)\right]\right.$$
$$\left.+5\sin\left[\sqrt{\frac{2}{3}g\Lambda^{1/3}-\frac{5}{48}}\left(\frac{1-(\Delta/\Lambda)^{1/6}}{1/6}\right)\right]\right\}.$$

Repeating the same procedure as in the $\alpha = 1/2$ scenario, we pick specific values of the chemical potential μ and expand the decaying portion of each of these the integrands around the maximum gap $\Delta = 1$. Then, integrating, we obtain the free energy behavior as a function of μ and Δ.

From the plot of $F(\Delta, \mu)$ for various μ we find that $\mu_c \approx 0.69$ (see fig.3.6). (The detail for $\Delta/\Delta_0 \sim 0.06$ is a non-physical mathematical artifact due to the IR boundary condition, and should be ignored.) In general, the behavior of the free energy here is essentially the same as in $\alpha = 1/2,\ \beta = 1$.

Appendix D

Conductance under Disorder

We assume the ballistic regime, i.e., $V \gg T, \gamma$.

Beginning with eq.(4.18),

$$S(V > T, \gamma) = \int_{1/t}^{\Lambda} \frac{d\omega}{\omega^2} \int d^2q \frac{g_\omega^2 \sqrt{\omega^2 - q^2}}{(\omega^2 - q^2) + g_\omega^2 q^2} = \int_{1/t}^{\Lambda} \frac{d\omega}{\omega} g_\omega^2 \int_0^1 dx \frac{\sqrt{1-x}}{1 - x + g_\omega^2 x} \tag{D.1}$$

where the coupling

$$g_\omega = \frac{g_0}{1 + \frac{g_0}{4} \ln \frac{\Lambda}{\omega}}, \qquad g_0 = e^2/v_F \approx 2 - 3. \tag{D.2}$$

This last term

$$S(t, g_0) = \frac{1}{4\pi} \int_{1/t}^1 \int_0^1 \frac{\sqrt{1-x}}{1 - x + x\frac{g_\omega^2}{16}} \left(\frac{g_\omega^2}{8}\right) \frac{1}{\omega} dx d\omega \tag{D.3}$$

whose solution,

$$\begin{aligned} S(t, g_0) = 2 &\frac{8\pi + g_0 \ln t}{\sqrt{[2\pi(4 - g_0) + g_0 \ln t]\,[2\pi(4 + g_0) + g_0 \ln t]}} \\ &\times \arctan\left[\frac{\sqrt{[2\pi(4 - g_0) + g_0 \ln t]\,[2\pi(4 + g_0) + g_0 \ln t]}}{2\pi g_0}\right]. \end{aligned} \tag{D.4}$$

To proceed further, we may approximate the above formula based upon the magnitude of the bare g_0. For both $g_0 \ll 1$ and $g_0 \sim 1$, we may approximate the above action by expanding the action around $\ln t \approx 0$. For example,

$$S(t, g_0 = 3) \approx \frac{8 \arctan\left(\sqrt{7}/3\right)}{\sqrt{7}} + \left(\frac{9}{7\pi} - \frac{27 \arctan\left(\sqrt{7}/3\right)}{7\pi\sqrt{7}}\right) \ln t \tag{D.5}$$

$$S(t, g_0 = 1) \approx \frac{8 \arctan\sqrt{15}}{\sqrt{15}} + \left(\frac{1}{15\pi} - \frac{\arctan\sqrt{15}}{15\pi\sqrt{15}}\right) \ln t \tag{D.6}$$

$$S(t, g_0 = 1/10) \approx 3.09255 + 0.000191373 \ln t. \tag{D.7}$$

Strictly speaking, the conductance (4.16) is, essentially,

$$G\,(V) \propto \int_1^\infty \frac{dt}{t^2} \cos(Vt) e^{-S(t)} \tag{D.8}$$

However, due to divergences, it is necessary to first compute

$$\frac{dG}{dV} \propto \int_1^\infty \frac{dt}{t} \sin(Vt) e^{-S(t)} \tag{D.9}$$

where t runs from 1 to infinity in units of $1/\Lambda$, where Λ is the maximum span of the Brillouin zone.

For $g_0 \gg 1$, we may follow the same procedure, expanding the action around $\ln t \approx 2$.

For $g_0 = 1$, the explicit solution

$$G(V) = -e^{-\frac{8 \arctan \sqrt{15}}{\sqrt{15}}} \int_0^V sgn(V') \times \left\{ \frac{225\pi \left|V'\right| \ {}_1F_2\left(\frac{1}{2} - \frac{1}{30\pi} + \frac{\arctan\sqrt{15}}{30\sqrt{15}\pi}; \frac{3}{2}, \frac{3}{2} - \frac{1}{30\pi} + \frac{\arctan\sqrt{15}}{30\sqrt{15}\pi}; -\frac{V'^2}{4}\right)}{225\pi + \sqrt{15}\arctan\sqrt{15} - 15} + \left|V'\right|^{\frac{15-\sqrt{15}\arctan\sqrt{15}}{225\pi}} \Gamma\left[\frac{\sqrt{15}\arctan\sqrt{15} - 15}{225\pi}\right] \times \sin\left[\frac{15 - \sqrt{15}\arctan\sqrt{15}}{450}\right] \right\} dV' \qquad \text{(D.10)}$$

where ${}_1F_2\left(a; b; z\right)$ is a hypergeometric function.

Appendix E

Feynman parameters

For two operators [96]

$$\frac{1}{AB} = \int_0^1 \frac{dx}{[(1-x)A + xB]^2} \tag{E.1}$$

Three...

$$\frac{1}{ABC} = 2\int_0^1 dx \int_0^x dy[Ay + B(x-y) + C(1-x)]^{-3} \tag{E.2}$$

In general, for two distinct operators [97],

$$\frac{1}{A^\alpha B^\beta} = \frac{\Gamma(\alpha+\beta)}{\Gamma(\alpha)\Gamma(\beta)} \int_0^1 dx \frac{x^{\alpha-1}(1-x)^{\beta-1}}{[Ax + B(1-x)]^{\alpha+\beta}}, \qquad (\alpha, \beta > 0) \tag{E.3}$$

$$\frac{1}{A_1 A_2 ... A_n} = \Gamma(n) \int_0^1 dx_1 \int_0^{x_1} dx_2 ... \int_0^{x_{n-2}} dx_{n-1} \times [A_1(1-x_1) + A_2(x_1 - x_2) + ... + A_n x_{n-1}]^{-n} \tag{E.4}$$

$$\frac{1}{A_1^{\alpha_1} A_2^{\alpha_2} ... A_n^{\alpha_n}} = \frac{\Gamma(\alpha_1 + ... + \alpha_n)}{\Gamma(\alpha_1)...\Gamma(\alpha_n)} \int_0^1 dx_1 \int_0^{x_1} dx_2 ... \int_0^{x_{n-2}} dx_{n-1} \times \frac{(1-x_1)^{\alpha_1 - 1}(x_1 - x_2)^{\alpha_2 - 1} ... x_{n-1}^{\alpha_n - 1}}{[A_1(1-x_1) + A_2(x_1 - x_2) + ... + A_n x_{n-1}]^{-(\alpha_1 + ... + \alpha_n)}}. \tag{E.5}$$

REFERENCES

[1] Y. Zhang, Y.-W. Tan, H. L. Stormer, and P. Kim, "Experimental observation of the quantum Hall effect and Berry's phase in graphene," Nature **438(10)**, 201 (2005).

[2] K. S. Novoselov, E. McCann, S. V. Morozov, V. I. Falko, M. I. Katsnelson, A. K. Geim, F. Schedin, and D. Jiang, "Unconventional quantum Hall effect and Berry's phase of 2π in bilayer graphene," Nature Physics **2**, 177 (2006).

[3] J. Gonzalez, F. Guinea, and M. A. H. Vozmediano, "Electron-electron interactions in graphene sheets," Phys. Rev. **B63**, 134 421 (2001).

[4] G. Semenoff, "Condensed-matter simulation of a three-dimensional anomaly," Phys. Rev. Lett. **53**, 2449 (1984).

[5] I. F. Herbut, "QED_3 theory of underdoped high-temperature superconductors," Phys. Rev. **B66**, 094 504 (2002).

[6] A. H. Castro-Neto, "Charge Density Wave, Superconductivity, and Anomalous Metallic Behavior in 2D Transition Metal Dichalcogenides," Phys. Rev. Lett. **86**, 4382 (2001).

[7] F. D. M. Haldane, "Model for a quantum Hall effect without Landau levels: Condensed-matter realization of the 'parity anomaly'," Phys. Rev. Lett. **61**, 2015 (1988).

[8] J. Gonzalez, F. Guinea, and M. A. H. Vozmediano, "Continuum approximation to fullerene molecules," Phys. Rev. Lett. **69**, 172 (1992).

[9] J. Gonzalez, F. Guinea, and M. A. H. Vozmediano, "Unconventional quasiparticle lifetime in graphite," Phys. Rev. Lett. **77**, 3589 (1996).

[10] J. Gonzalez, F. Guinea, and M. A. H. Vozmediano, "The Electronic Spectrum of Fullerenes from the Dirac Equation," Nucl. Phys. **B406**, 771 (1993).

[11] J. Gonzalez, F. Guinea, and M. A. H. Vozmediano, "Non-Fermi liquid behavior of electrons in the half-filled honeycomb lattice (A renormalization group approach)," Nucl. Phys. **B424**, 595 (1994).

[12] J. Gonzalez, F. Guinea, and M. A. H. Vozmediano, "Marginal-Fermi-liquid behavior from two-dimensional Coulomb interaction," Phys. Rev. **B59**, 2474 (1999).

[13] T. Stauber, F. Guinea, and M. A. H. Vozmediano, "Disorder and interaction effects in two-dimensional graphene sheets," Phys. Rev. **B71**, 041 406(R) (2005).

[14] M. S. Dresselhaus, G. Dresselhaus, and P. C. Eklund, *Science of Fullerenes and Carbon Nanotubes* (Academic, 1996).

[15] M. S. Dresselhaus, G. Dresselhaus, , and P. Avouriseds.,, *Carbon Nanotubes* (Springer-Verlag, 2001).

[16] E. Rollings, G.-H. Gweon, S. Y. Zhou, B. S. Mun, B. S. Hussain, A. V. Fedorov, P. N. First, W. A. de Heer, and A. Lanzara, "Synthesis and characterization of atomically-thin graphite films on a silicon carbide substrate," unpublished (2005).

[17] J. Hass, C. A. Jeffrey, R. Feng, T. Li, X. Li, Z. Song, C. Berger, W. A. de Heer, P. N. First, and E. H. Conrad, "Highly-ordered graphene for two dimensional electronics," unpublished (2006).

[18] Y. Zhang, J. P. Small, W. V. Pontius, and P. Kim, "Fabrication and Electric Field Dependent Transport Measurements of Mesoscopic Graphite Devices," unpublished (2004).

[19] K. S. Novoselov, A. K. Geim, S. V. Morozov, D. Jiang, M. I. Katsnelson, I. V. Grigorieva, S. V. Dubonos, and A. A. Firsov, "Two-dimensional gas of massless Dirac fermions in graphene," Nature **438**, 197 (2005).

[20] Y. Zhang, Z. Jiang, J. P. Small, M. S. Purewal, Y.-W. Tan, M. Fazlollahi, J. D. Chudow, J. A. Jaszczak, H. L. Stormer, and P. Kim, "Landau-Level Splitting in Graphene in High Magnetic Fields," Phys. Rev. Lett. **96**, 136 806 (2006).

[21] K. S. Novoselov, A. K. Geim, S. V. Morozov, D. Jiang, Y. Zhang, S. V. Dubonos, I. V. Grigorieva, and A. A. Firsov, "Room-temperature electric field effect and carrier-type inversion in graphene films," Science **306 (5696)**, 666 (2004).

[22] C., Z. Song, T. Li, X. Li, A. Y. Ogbazghi, R. Feng, Z. Dai, A. N. Marchenkov, E. H. Conrad, P. N. First, and W. A. de Heer, "Ultrathin Epitaxial Graphite: 2D Electron Gas Properties and a Route toward Graphene-based Nanoelectronics," J. Phys. Chem. **B108**, 19 912 (2004).

[23] Y. Zhang, J. P. Small, M. E. S. Amori, and P. Kim, "Electric Field Modulation of Galvanomagnetic Properties of Mesoscopic Graphite," Phys. Rev. Lett. **94**, 176 803 (2005).

[24] G. P. Mikitik and Y. V. Sharlai, "Manifestation of Berry's phase in metal physics," Phys. Rev. Lett. **82**, 2147 (1999).

[25] Y. Zheng and T. Ando, "Hall conductivity of a two-dimensional graphite system," Phys. Rev. **B 65**, 245 420 (2002).

[26] V. P. Gusynin and S. G. Sharapov, "Unconventional integer quantum Hall effect in graphene," Phys. Rev. Lett. **95**, 146 801 (2005).

[27] N. M. R. Peres, F. Guinea, and A. H. Castro-Neto, "Electronic properties of Disordered Two-Dimensional Carbon," Phys. Rev. **B73**, 125 411 (2006).

[28] M. L. Sadowski, G. Martinez, M. Potemski, C. Berger, and W. A. de Heer, "Landau level spectroscopy of ultrathin graphite layers," unpublished (2006).

[29] B. A. Volkov, Y. V. Kopaev, and A. I. Rusinov, "Theory of 'excitonic' ferromagnetism," Sov. Phys. JETP **41**, 952 (1975).

[30] B. A. Volkov, A. I. Rusinov, and R. K. Timerov, "Phase diagram of an excitonic ferromagnet at finite temperatures," Sov. Phys. JETP **43**, 589 (1976).

[31] M. E. Zhitomirsky, T. M. Rice, and V. I. Anisimov, "Magnetic properties: Ferromagnetism in the hexaborides," Nature **402**, 251 (1999).

[32] V. Barzykin and L. P. Gorkov, "Ferromagnetism and Superstructure in Ca1xLaxB6," Phys. Rev. Lett. **84**, 2207 (2000).

[33] L. Balents and C. M. Varma, "Ferromagnetism in Doped Excitonic Insulators," Phys. Rev. Lett. **84**, 1264 (2000).

[34] E. Bascones, A. A. Burkov, and A. H. MacDonald, "Theory of Ferromagnetism in Doped Excitonic Condensates," Phys. Rev. Lett. **89**, 086 401 (2002).

[35] L. Balents, "Excitonic order at strong coupling: Pseudospin, doping, and ferromagnetism," Phys. Rev. **B62**, 2346 (2000).

[36] M. Y. Veillette and L. Balents, "Weak ferromagnetism and excitonic condensates," Phys. Rev. **B65**, 014 428 (2002).

[37] M. C. Bennett, J. van Lierop, E. M. Berkeley, J. F. Mansfield, C. Henderson, M. C. Aronson, D. P. Young, A. Bianchi, Z. Fisk, F. Balakirev, and A. Lacerda, "Weak ferromagnetism in CaB_6," Phys. Rev. **B69**, 132 407 (2004).

[38] D. A. Abanin, P. A. Lee, and L. S. Levitov, "Spin Filtered Edge States and Quantum Hall Effect in Graphene," Phys. Rev. Lett. **96**, 176 803 (2006).

[39] D. V. Khveshchenko, "Ghost Excitonic Insulator Transition in Layered Graphite," Phys. Rev. Lett. **87**, 246 802 (2001).

[40] D. V. Khveshchenko and W. F. Shively, "Excitonic pairing between nodal fermions," Phys. Rev. **B73**, 115 104 (2006).

[41] E. V. Gorbar, V. P. Gusynin, V. A. Miransky, and I. A. Shovkovy, "Magnetic field driven metal-insulator phase transition in planar systems," Phys. Rev. **B66**, 045 108 (2002).

[42] A. L. Tchougreeff and R. Hoffmann, "Charge and spin density waves in the electronic structure of graphite: Application to analysis of STM images," J. Phys. Chem. **96**, 8993 (1992).

[43] F. R. Wagner and M. B. Lepetit, "Symmetry-Broken HF Solutions for Graphite Surfaces," J. Phys. Chem. **100**, 11 050 (1996).

[44] S. Xu, J. Cao, C. C. Miller, D. A. Mantell, R. J. D. Miller, and Y. Gao, "Energy dependence of electron lifetime in graphite observed with femtosecond photoemission spectroscopy," Phys. Rev. Lett. **76**, 483 (1996).

[45] K. Ertel, U. Kohl, J. Lehmann, M. Merschdorf, W. Pfeiffer, A. Thon, S. Voll, and G. Gerber, "Time-resolved two-photon photoemission spectroscopy of HOPG and Ag nanoparticles on HOPG," Appl. Phys. **B 68**, 439 (1999).

[46] D. V. Khveshchenko and H. Leal, "Excitonic instability in layered degenerate semimetals," Nucl. Phys. **B687**, 323 (2004).

[47] R. Haslinger and A. V. Chubukov, "Condensation energy in strongly coupled superconductors," Phys. Rev. **B67**, 140 504 (2003).

[48] R. Haslinger and A. V. Chubukov, "Condensation energy in strongly coupled superconductors," Phys. Rev. **B68**, 214 508 (2003).

[49] E. Tsoncheva and A. V. Chubukov, "Condensation energy in Eliashberg theory: From weak to strong coupling," Phys. Rev. **B71**, 184 513 (2005).

[50] E. Tsoncheva and A. V. Chubukov, "Erratum: Condensation energy in Eliashberg theory: From weak to strong coupling," Phys. Rev. **B72**, 149 902 (2005).

[51] E. V. Gorbar, V. P. Gusynin, V. A. Miransky, and I. A. Shovkovy, "Fractal structure of the effective action in (quasi)planar models with long-range interactions," Phys. Lett. **A313**, 472 (2003).

[52] T. Appelquist, D. Nash, and L. Wijewardhana, "Critical behavior in (2+1)-dimensional QED," Phys. Rev. Lett. **60**, 2575 (1988).

[53] T. Appelquist, J. Terning, and L. Wijewardhana, "(2+1)-dimensional QED and a novel phase transition," Phys. Rev. Lett. **75**, 2081 (1995).

[54] T. Appelquist, A. G. Cohen, and M. Schmaltz, "A new constraint on strongly coupled field theories," Phys. Rev. **D60**, 045 003 (1999).

[55] D. V. Khveshchenko, "Magnetic-Field-Induced Insulating Behavior in Highly Oriented Pyrolitic Graphite," Phys. Rev. Lett. **87**, 206 401 (2001).

[56] D. V. Khveshchenko, "Coulomb interacting Dirac fermions in disordered graphene," unpublished (2006).

[57] M. A. H. Vozmediano, M. P. López-Sancho, T. Stauber, and F. Guinea, "Local defects and ferromagnetism in graphene layers," Phys. Rev. **B 72**, 155 121 (2005).

[58] N. M. R. Peres, F. Guinea, and A. H. Castro-Neto, "Coulomb interactions and ferromagnetism in pure and doped graphene," Phys. Rev. **B 72**, 174 406 (2005).

[59] N. M. R. Peres, F. Guinea, and A. H. Castro-Neto, "Electronic properties of disordered two-dimensional carbon," Phys. Rev. **B 73**, 125 411 (2006).

[60] J. Nilsson, A. H. Castro-Neto, N. M. R. Peres, and F. Guinea, "Electron-electron interactions and the phase diagram of a graphene bilayer," Phys. Rev. **B 73**, 214 418 (2006).

[61] L. Levitov and A. Shytov, "Semiclassical theory of the Coulomb anomaly," JETP Lett. **66**, 214 (1997).

[62] P. Kopietz, "Coulomb Gap in the Density of States of Disordered Metals in Two Dimensions," Phys. Rev. Lett. **81**, 2120 (1998).

[63] B. L. Altshuler and A. G. Aronov, *ElectronElectron Interactions in Disordered Systems*, Vol. 10 of Modern Problems in Condensed Matter Systems, A. L. Efros and M. Pollak, eds. (North-Holland, 1985).

[64] B. L. Altshuler and A. G. Aronov, Sov. Phys. JETP **50**, 968 (1979).

[65] B. L. Altshuler and A. G. Aronov, "Zero bias anomaly in tunnel resistance and electron-electron interaction," Solid State Communications **30**, 115 (1979).

[66] B. L. Altshuler, A. G. Aronov, and P. A. Lee, "Interaction effects in disordered Fermi systems in two dimensions," Phys. Rev. Lett. **44**, 1288 (1980).

[67] A. M. Rudin, I. L. Aleiner, and L. I. Glazman, "Tunneling zero-bias anomaly in the quasiballistic regime," Phys. Rev. **B55:15**, 9322 (1997).

[68] D. V. Khveshchenko and M. Reizer, "Effects of two-dimensional plasmons on the tunneling density of states," Phys. Rev. **B57**, R4245 (1998).

[69] E. G. Mishchenko and A. V. Andreev, "Zero-bias anomaly in two-dimensional electron layers and multiwall nanotubes," Phys. Rev. **B65**, 235 310 (2002).

[70] C. Bena and S. A. Kivelson, "Quasiparticle scattering and local density of states in graphite," Phys. Rev. **B 72**, 125 432 (2005).

[71] V. M. Pereira, F. Guinea, J. M. B. L. dos Santos, N. M. R. Peres, and A. H. Castro-Neto, "Disorder Induced Localized States in Graphene," Phys. Rev. Lett. **96**, 036 801 (2006).

[72] Y. G. Pogorelov, "Anomalous impurity resonance in graphene," unpublished (2006).

[73] P. J. Hirschfeld and W. A. Atkinson, "Π à la Node: Disordered d-Wave Superconductors in Two Dimensions for the Random Masses," J. Low Temp. Phys. **126**, 881 (2002).

[74] Y. V. Nazarov, JETP Lett. **68**, 561 (1989).

[75] A. Kamenev and A. V. Andreev, "Electron-electron interactions in disordered metals: Keldysh formalism," Phys. Rev. **B60**, 2218 (1999).

[76] L. Bartosch and P. Kopietz, "Zero bias anomaly in the density of states of low-dimensional metals," Eur. Phys. J. **B28**, 29 (2002).

[77] P. Jiang, I. Yang, W. Kang, L. N. Pfeiffer, K. W. Baldwin, and K. W. West, "Interaction Effects and Pseudogap in Two-Dimensional Lateral Tunnel Junctions," unpublished (2006).

[78] D. V. Khveshchenko and J. Paaske, "Incipient Nodal Pairing in Planar d-wave Superconductors," Phys. Rev. Lett. **86**, 4672 (2001).

[79] M. Vojta, Y. Zhang, and S. Sachdev, "Quantum Phase Transitions in d-Wave Superconductors," Phys. Rev. Lett. **85**, 4940 (2000).

[80] D. H. Kim and P. A. Lee, "Theory of Spin Excitations in Undoped and Underdoped Cuprates," Annals of Physics **272**, 130 (1999).

[81] I. F. Herbut, "Antiferromagnetism from Phase Disordering of a d-Wave Superconductor," Phys. Rev. Lett. **88**, 047 006 (2002).

[82] Z. Tesanovic, O. Vafek, and M. Franz, "Chiral symmetry breaking and phase fluctuations: A QED_3 theory of the pseudogap state in cuprate superconductors," Phys. Rev. **B65**, 180 511 (2002).

[83] M. Franz, D. E. Sheehy, and Z. Tesanovic, "Magnetic Field Induced Charge and Spin Instabilities in Cuprate Superconductors," Phys. Rev. Lett. **88**, 257 005 (2002).

[84] A. Puchkov, D. Basov, and T. Timusk, "The pseudogap state in high-T_c superconductors: an infrared study," J. Phys. Cond. Matter **8**, 10 049 (1996).

[85] A. Abanov, A. V. Chubukov, and A. M. Finkelstein, "Coherent vs. incoherent pairing in 2D systems near magnetic instability," Europhys. Lett. **54**, 488 (2001).

[86] D. J. Scalapino, "The case for $d_{x^2-y^2}$ pairing in the cuprate superconductors," Phys. Rep. **250**, 329 (1995).

[87] D. Pines, Z. Phys. B **103**, 129 (1997).

[88] A. Chubukov, "Theory of the leading edge gap in underdoped cuprates," Europhys. Lett. **44**, 655 (1998).

[89] A. Chubukov and J. Schmalian, "Temperature variation of the pseudogap in underdoped cuprates," Phys. Rev. **B 57**, R11 085 (1998).

[90] A. Abanov and A. Chubukov, "A Relation between the Resonance Neutron Peak and ARPES Data in Cuprates," Phys. Rev. Lett. **83**, 1652 (1999).

[91] A. Abanov, A. V. Chubukov, and J. Schmalian, "Quantum-critical superconductivity in underdoped cuprates," Europhys. Lett. **55**, 369 (2001).

[92] A. V. Chubukov and J. Schmalian, "Strong coupling superconductivity due to massless boson exchange," submitted to Phys. Rev. B .

[93] J. Mesot, M. R. Norman, H. Ding, M. Randeria, J. C. Campuzano, A. Paramekanti, H. M. Fretwell, A. Kaminski, T. Takeuchi, T. Yokoya, T. Sato, T. Takahashi, T. Mochiku, and K. Kadowaki, "Superconducting Gap Anisotropy and Quasiparticle Interactions: a Doping Dependent ARPES Study," Phys. Rev. Lett. **83**, 840 (1999).

[94] R. Gatt, S. Christensen, B. Frazer, Y. Hirai, T. Schmauder, R. J. Kelley, M. Onellion, I. Vobornik, L. Perfetti, G. Margaritondo, A. Morawski, T. Lada, A. Paszewin, and C. Kendziora, "Superconducting Gap vs. Wave Vector: Evidence for Hot Regions on the Fermi Surface," unpublished (1999).

[95] V. A. Miransky, *Dynamical Symmetry Breaking in Quantum Field Theories* (World Scientific, Singapore, 1993).

[96] S. Weinberg, *The Quantum Theory of Fields*, Vol. 1 (Cambridge, 1995).

[97] D. Bailin and A. Love, *Introduction to Gauge Field Theory (Graduate Student Series in Physics)* (Taylor and Francis, 1993), revised edn.